The Journal of Chemical Thermodynamics, Volume 158, 2021, 106434. https://doi.org/10.1016/j.jct.2021.106434

Speed of sound and phase equilibria for (CO_2 + C_3H_8) mixtures

Daniel Lozano-Martín[a]; Rodrigo Susial[a], Pedro Hernández[a,b] Teresa E. Fernández-Vicente[c], M. Carmen Martín[a], José J. Segovia[a,*]

[a] TERMOCAL Research Group, Research Institute on Bioeconomy, Escuela de Ingenierías Industriales, Universidad de Valladolid, Paseo del Cauce, 59, 47011 Valladolid, Spain.

[b] Instituto Nacional de Técnica Aeroespacial (INTA), 28850 Torrejón de Ardoz, Madrid, Spain

[c] Centro Español de Metrología (CEM), Alfar 2, 2876 Tres Cantos, Madrid, Spain.

* Corresponding author e-mail: jose.segovia@eii.uva.es

Abstract

This work presents phase envelope and speed of sound data for the (0.60 CO_2 + 0.40 C_3H_8) and (0.80 CO_2 + 0.20 C_3H_8) binary mixtures. Phase equilibria was measured using a cylindrical resonator working in the microwave band whereas an acoustic resonator was used for speed of sound measurements. The experimental results were compared GERG-2008 equation of state, obtaining average absolute deviations by 0.24% in pressure for phase equilibria data and 0.025% for speed of sound data. Speed of sound values were used to derive perfect-gas heat capacities, acoustic virial coefficients and second density virial coefficients. In addition, AGA8-DC92 EoS performance was checked for the results derived from speeds of sound.

Keywords: speed of sound; phase equilibria; carbon dioxide; propane; heat capacities as perfect-gas; acoustic virial coefficients; density virial coefficients.

1. Introduction.

Several uses have been analyzed for carbon dioxide + propane mixtures. Some authors have proposed and studied these mixtures as natural mixtures with low global warming and zero ozone depletion potentials for substitution of classical refrigerants [1,2]. Other researches have explored the application of these mixtures as non-toxic and non-flammable fluid for power generation by organic Rankine cycles of low-grade heat [3,4]. This binary system is also used as solvent in supercritical phase for the extraction of oils from seeds and for the hydrogenation of vegetable oils and fats, due to the improvement in the mass transfer rates and reduction in the amount of reactant required and undesirable by-products [5–8]. Furthermore, it has attracted interest as working fluid for enhanced oil recovery methods by its injection into specific heavy oil reservoirs [9]. All studies agree that accurate knowledge of the thermophysical properties for these mixtures is required.

The reference thermodynamic model for these mixtures is the GERG-2008 equation of state (EoS) [10,11], originally developed for natural gas-like mixtures. The application range is limited to mole fractions $x_{CO_2} \leq 0.30$ and $x_{C_3H_8} \leq 0.14$ in the intermediate quality range, covering the pressure range p = (0 - 35) MPa and temperature range T = (90 - 450) K in the normal range. The binary interaction between carbon dioxide and propane is fitted to selected (p,ρ,T), saturated liquid density and vapor-liquid equilibrium data, but the quality and extension of the experimental data sets is not sufficient for the development of a departure function, thus the interactions are only adjusted through the reducing functions. Apart from the recommendation of the development of a new specific departure function for mixtures of (CO_2 + C_3H_8) when comprehensive and accurate data are available, GERG-2008 report [10,11] indicates also the necessity of further measurements for improving the data situation for caloric properties for this system. This is because the only speed of sound measurements founded in the literatures are those of Lin et al. [12], restricted to mole fractions $x_{C_3H_8} \leq 0.938$. The covered range in composition is constrained to a very low-range in the liquid and

supercritical phase because the goal at this research is the use of propane as a doping impurity for the catalytic inhibition of the vibrational relaxation phenomena that causes a large sound absorption and dispersion in pure carbon dioxide, which prevents the accurate study of the speed of sound with typical acoustic cavities at high frequency.

Thus, the present work focus on the study of the speed of sound and phase equilibria of two mixtures of nominal molar compositions (0.60 CO_2 + 0.40 C_3H_8) and (0.80 CO_2 + 0.20 C_3H_8). Mixtures with a composition around mole fraction x_{C3H8} = 0.3 since, at this composition, the mixture reaches the limit of flammability and is usually chosen as optimum for the afore-mentioned applications.

Speed of sound measurements are performed with one of the state-of-art techniques, the spherical acoustic resonator, are compared to the GERG-2008 EoS [10,11] and to AGA8-DC92 EoS [13,14] which is already widely used in the industry in order to check the uncertainty of these models. In addition, the perfect-gas isochoric and isobaric heat capacities, along with the acoustic virial coefficients are derived from the speed of sound data to assist in the development of future reliable correlations for improving the thermodynamic models. The density second virial coefficients have been determined from the acoustic ones to provide a robust interpretation of the speed of sound measurements and further comparison with the literature. Finally, phase equilibria were also determined using a microwave cylindrical resonator, recently developed in our laboratory [15].

2. Materials and Methods.

2.1 Mixtures.

Two binary (CO_2 + C_3H_8) mixtures were prepared at the Spanish Center of Metrology (CEM) in Madrid, Spain, according to the standard gravimetric procedure described in the ISO 6142-1 [16] and ISO 6143 [17]. Supplier, purity, molar mass and critical parameters of the pure

gases used in the preparation are reported in Table which also contains composition and corresponding expanded ($k = 2$) uncertainty for the two mixtures. Carbon dioxide and propane were used without further purification, but their impurities were considered in the mixture preparation and taken into account in the reported uncertainty of the composition. The mixtures were homogenized by heating and rolling and checked by gas chromatography (GC), with differences between gravimetric composition and GC analysis within uncertainties.

Table 1. Purity, supplier, critical parameters of the pure components used for preparation of the binary (CO_2 + C_3H_8) mixtures at CEM, molar composition x_i and expanded (k = 2) uncertainty $U(x_i)$ of the binary (CO_2 + C_3H_8) mixtures studied in this work.

	Supplier	Purity / mol fraction[b]	CAS number	M / g·mol^{-1}	Critical parameters[a]	
					T_c / K	p_c / MPa
Carbon Dioxide	Air Liquide	≥ 0.99998	124-38-9	44.010	304.13	7.3773
Propane	Air Liquide	≥ 0.99950	74-98-6	44.096	369.89	4.2512

Components	(0.60 CO_2 + 0.40 C_3H_8)			(0.80 CO_2 + 0.20 C_3H_8)		
	$10^2 \cdot x_i$ / mol/mol	$10^2 \cdot U(x_i)$ / mol/mol	Impurities	$10^2 \cdot x_i$ / mol/mol	$10^2 \cdot U(x_i)$ / mol/mol	Impurities
Carbon Dioxide	60.059	0.029	≤ 80 parts in 10^6 of other hydrocarbons	80.110	0.015	≤ 40 parts in 10^6 of other hydrocarbons
Propane	39.941	0.021		19.890	0.011	

(a) Critical parameters were obtained by using the default equation for each substance in REFPROP software [18], the reference equation of state for carbon dioxide [19] and the reference equation of state for propane [20].

[b] The stated purities were provided by the suppliers.

2.2 Experimental techniques.

2.2.1 Acoustic spherical resonator.

A schematic diagram of the experimental apparatus, for measuring speeds of sound, is depicted in Figure 1.

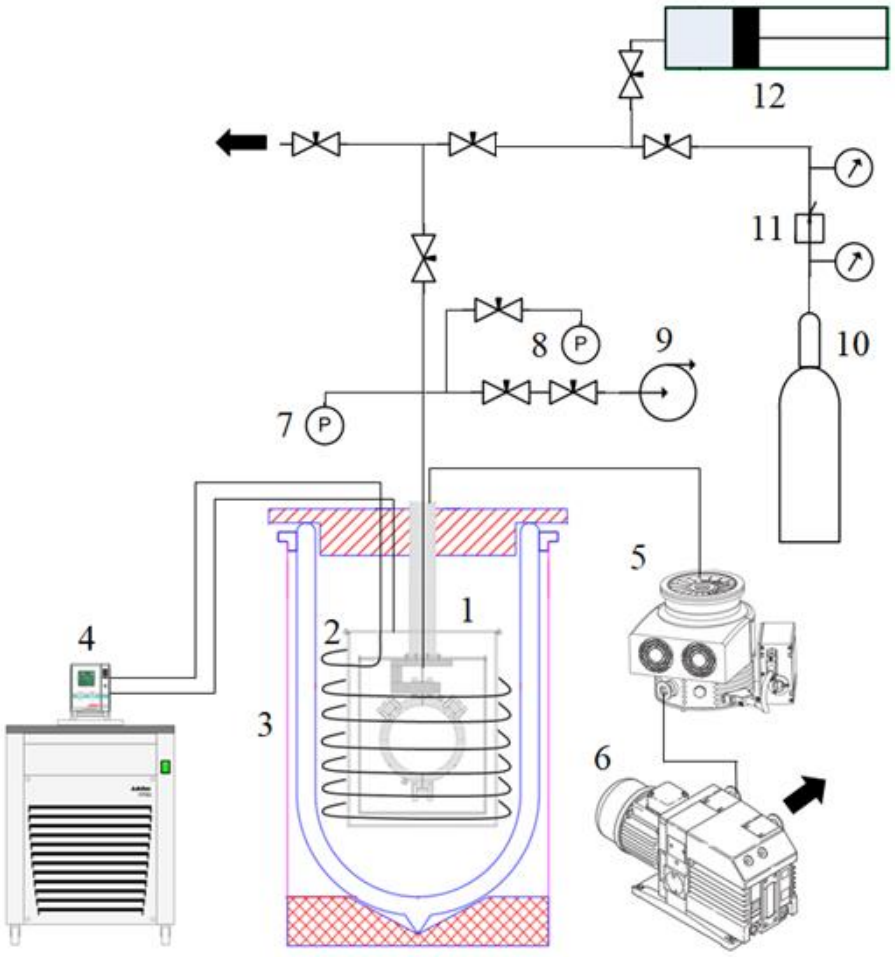

Figure 1. Schematic diagram of the technique for measuring speeds of sound: 1. Acoustic cavity; 2. Cooling coil; 3. Ethanol Dewar; 4. Cooling bath; 5. Turbomolecular pump; 6. Centrifugal pump; 7. pressure transducer (up to 20 MPa); 8. pressure transducer (up to 2 MPa); 9. Vacuum pump; 10. Gas sample bottle; 11. Pressure regulator; 12. Hand operated piston pump.

The setup comprises the spherical acoustic resonator of 40 mm internal radius in A321-type stainless-steel, designed to operate at pressures and temperatures up to 20 MPa and 475 K, which serves as acoustic cavity and pressure-tight vessel. An internal and an external stainless-steel shells, provided with a shield of aluminum over fibber-glass and under vacuum inside, prevent heat losses by radiation and convection. A cooled ethanol Dewar fed by a stirred thermal bath (FP89, Julabo) is used to maintain the system around ten degrees below the desire temperature and the cavity is heated by conduction using several electrical heaters around the internal shell. A gas manifold was designed to fill and evacuate the resonator with the gas sample from the bottle using a hand-operated gas piston and a vacuum pump (Trivac D8B, Leybold). More details about the construction and calibration of the internal radius of the cavity, by acoustic measurements in pure argon, were presented in previous works [21-22].

Acoustic signal is generated inside the cavity by a capacitance-type acoustic transducer made ad-hoc for this technique powered by an ac signal from a wave synthesizer (3225B, HP) without bias voltage. Acoustic wave is detected at twice the driven frequency by other equal capacitance transducer externally polarized with 80 DCV with a Lock-In amplifier (SR850 DSP, SRS) operating at differential voltage mode and referenced to the wave generator. Phase sensitive detection, performed by the Lock-In, decomposes the received signal into two components, the in-phase "*u*" and the quadrature "*v*", which are interpolated to a Lorentzian shape function of frequency *f* of wave generator [23,24]:

$$u + iv(f) = \frac{iAf}{(F^2 - f^2)} + B + C(f - f_{0n}) \qquad (1)$$

with $F = f_{0n} + ig_{0n}$, where f_{0n} stands for resonance frequency and g_{0n} stands for resonance halfwidth of the radial acoustic modes (0,*n*) and *A*, *B*, and *C* are complex parameters. Typical acoustic pressure levels of (1 to 20) mPa are generated, which produce signal amplitudes

between (10 to 200) μV. More information about the design of acoustic transducers and acquisition instrumentation and procedures used for determination of the resonance acoustic signal were described elsewhere [25–27].

Temperature is determined as the mean of the readings of two 25.5 Ω standard platinum resistance thermometers (162D, Rosemount) plugged to an ac resistance bridge (F18, ASL) which are calibrated on the international temperature scale ITS-90 [28,29]. They are located in the northern and southern hemispheres of the acoustic cavity and the overall expanded (k = 2) uncertainty in temperature is better than 5 mK. Pressure is measured by two piezoelectric quartz transducers (Digiquartz 2003A-101, Paroscientific) for pressures from (0 to 2) MPa and (Digiquartz 43KR-101, Paroscientific) for pressures up to 20 MPa. They are calibrated against a dead-weight balance and the overall expanded (k = 2) in pressure is between (220 to 380) Pa for the explored range in this work.

Resonance frequencies f_{0n} of the first five radial acoustic (0,n) modes are recorded from the highest measuring pressure and decreased in several steps down to nearly 0.1 MPa, obtaining about 8 to 11 points per isotherm for each mixture.

The purely radial modes (0,n) are preferred due to their motion is normal to the wall of the resonance cavity, thus they are not affected by the viscous boundary layer and, in addition, they exhibit less sensitivity to imperfections of the geometry of the cavity.

The maximum measured pressure was set to 75 % of the saturation pressure p_{sat} for those isotherms below the phase envelope to avoid the dispersion and absorption effects of precondensation on the speed of sound measurements [30]. This affects the isotherms T = (273.16, 300, and 325) K for the mixture (0.60 CO_2 + 0.40 C_3H_8) with p_{sat} = (1.17, 2.58 and 5.27) MPa, respectively, and isotherms T = (273.16 and 300) K for the mixture (0.80 CO_2 + 0.20 C_3H_8) with p_{sat} = (2.16 and 4.79) MPa, respectively. For the rest of temperatures, the amount of gas available in the sampling bottles limits the achievable pressure after several

loads with the gas piston. On the other hand, the lowest pressure was chosen by the experience, as a compromise between a sufficiently low measuring state to get good accuracy when deriving the properties in the limit of zero pressure from the acoustic data, but with a resonance halfwidth not too wide that increases the fitting error of the resonance frequency to Equation (1).

Each measuring point consists of several repetitions of the acoustic resonance frequency f_{0n} and halfwidth g_{0n}, the former are converted to their equivalent values at the reference temperatures T from the experimental ones T_{exp} using the estimated speed of sound $w(p,T)$ and $w(p,T_{exp})$ from REFPROP 10 [18] by:

$$f_{0n}(p,T) = f_{0n}(p,T_{exp})\left(w(p,T) \Big/ w(p,T_{exp}) \right) \tag{2}$$

and then, averaged to a single mean estimate of f_{0n} and g_{0n}, to obtain the experimental speed of sound $w_{0n}(p,T)$ at the desired temperature T and pressure p for every mode and every mixture by:

$$w_{0n}(p,T) = \frac{2\pi a}{\nu_{0n}}\left(f_{0n} - \Delta f \right) \tag{3}$$

where $a = a(p,T)$ is the internal radius of the cavity and ν_{0n} is the zero of spherical Bessel first derivative of every n^{th} mode. Δf stands for the frequency correction, which is the sum of the frequency perturbations produced by different effects. Standard models were considered for the application of Δf to our data sets, whose concrete expressions used in this work are specified elsewhere [31]. The overall frequency correction extends from −29 parts in 10^6 at p = 0.5 MPa, T = 325 K, mode (0,6) for the (0.60 CO_2 + 0.40 C_3H_8) mixture until −107 parts in 10^6 at p = 0.12 MPa, T = 325 K, mode (0,2) for the (0.80 CO_2 + 0.20 C_3H_8) mixture. The most significate contribution can be as high as −70 parts in 10^6 from the thermal boundary layer perturbation, with a relatively small magnitude at the highest pressures of −40 parts in 10^6

from the correction of the coupling of gas and shell motion due to the low value of the speed of sound for these mixtures, and non-depreciable terms from the ducts perturbation ranging from +10 to −25 parts in 10^6.

Finally, perturbation on the acoustic resonance frequency and contribution to the halfwidth due to the relaxation phenomena was also assessed. It is already known that small rigid polyatomic molecules, such as carbon dioxide, exhibits long vibrational relaxations times τ that produces high absorption and dispersion of the sound wave [32–34]. On the contrary, more complex molecules such as propane have so small vibrational relaxation times τ that this effect is negligible [35–37]. At low densities, τ can be assumed as inversely proportional to the density, and for the case of mixtures of carbon dioxide (component 1) and propane (component 2), the vibrational relaxation time associated to like collisions of carbon dioxide molecules τ_{11} at ρ = 1 mol·m^{-3} decrease from (280 to 180) μs in the temperature range of this research [32], while a more effective relaxation happens between unlike collisions of carbon dioxide and propane, with associated vibrational relaxation times τ_{12} about two orders of magnitude lower than τ_{11} [12,38].

Under the assumption that all carbon dioxide and propane molecules relax at unison following a parallel process each defined by a single relaxation time τ_k, such that $\tau_k^{-1} = x_k/\tau_{kk} + x_j/\tau_{kj}$ is the vibrational relaxation time of molecule k as a consequence of collisions between like molecules τ_{kk} and unlike molecules τ_{kj}, the effect of the vibrational relaxation for carbon dioxide is clearly reduced due to the addition of propane. This is also reflected in the magnitude of the relative excess halfwidths, defined as $\Delta g_{0n}/f_{0n} = g_{exp} - (g_{th} + g_0 + g_{bulk})/f_{0n}$, where g_{th} stands for the contribution to the halfwidth of the thermal boundary layer, g_0 stands for the contribution to the halfwidth of the gas ducts, and g_{bulk} stands for the viscothermal dissipation in the bulk of the fluid: the $\Delta g_{0n}/f_{0n}$ of pure carbon dioxide reported in the literature [32] is as high as 1200 parts in 10^6 at the lowest experimental pressures reported of 0.4 MPa before allowance for vibrational relaxation, one order of magnitude larger than the 150 parts

in 10^6 for the higher mode (0,6) at the same state according to our values displayed in Figure 2.

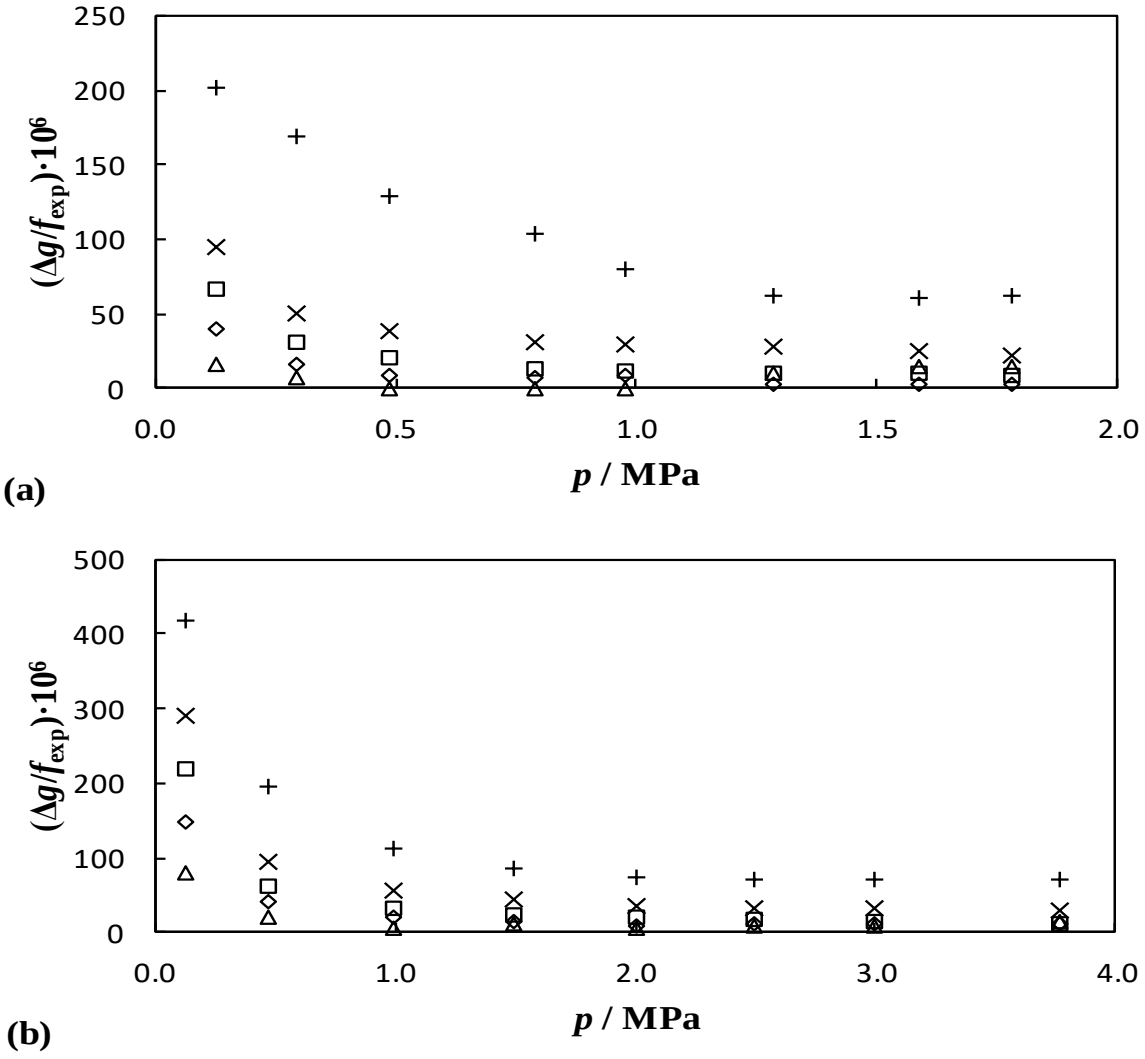

Figure 2. Relative excess halfwidths $(\Delta g/f)_{0n}$ for (a) the (0.60 CO_2 + 0.40 C_3H_8) mixture and (b) for the (0.80 CO_2 + 0.20 C_3H_8) mixture at T = 375 K and modes △ (0,2), ◇ (0,3), □ (0,4), × (0,5), ＋ (0,6).

However, the excess halfwidth increasing trend as decreasing pressure indicates that some vibrational relaxation is taking place in our experiment. Following the procedure described by Estela-Uribe et al. [39], according to which the contribution to the halfwidths g_{vib} and the corresponding frequency perturbation Δf_{vib} by vibrational relaxation on leading order are:

$$\frac{g_{\text{vib}}}{f} = \frac{\Delta g}{f} = \pi(\gamma - 1) f \left[\Delta_1 \tau_1 + \frac{\Delta_2 \tau_2}{1 + (2\pi f \tau_2)^2} \right] \tag{4}$$

$$\begin{aligned} \frac{\Delta f_{\text{vib}}}{f} = {} & \frac{1}{2}(\gamma - 1)\left[1 - \frac{\Delta_1 (1 + 3\gamma)}{4} \right] \Delta_1 (2\pi f \tau_1)^2 \\ & + \frac{1}{2}(\gamma - 1)\left[\frac{1}{1 + (2\pi f \tau_2)^2} \right] \Delta_2 (2\pi f \tau_2)^2 \end{aligned} \tag{5}$$

where $\Delta_k = x_k C_{\text{vib},k}/C_{\text{p,m}}$ is the vibrational contribution C_{vib} to the molar isobaric heat capacity of the mixture $C_{\text{p,m}}$, with values of $\Delta_1 \geq 7 \cdot 10^{-2}$ and $\Delta_2 \geq 12 \cdot 10^{-2}$ and, therefore, with a significant contribution of the relaxation of both carbon dioxide and propane molecules at all the temperatures of this work. C_{vib} was obtained from Plank-Einstein functions $C_{\text{vib}} = R \sum_i \frac{z_i^2 e^{z_i}}{(e^{z_i} - 1)^2}$ with $z_i = (h_P \cdot \nu_i)/(k_B \cdot T)$ where h_P stands for the Planck constant, k_B stands for the Boltzmann constant, and ν_i are the *i*-th experimental vibrational frequency obtained from spectroscopy techniques for pure carbon dioxide [40] and propane [41]. Unfortunately, we have obtained really disparate results, with very small values of $\tau_{12} \cdot \rho \leq 10^{-10}$ s·(mol·m^{-3}) and very large values of $\tau_{21} \cdot \rho \geq 10$ s·(mol·m^{-3}), which suggest that the proposed model and assumptions are not suitable for the interpretation of the present data.

In any case, taken into account that the mode (0,6) is the only mode whose excess halfwidth Δg_{06} is higher than $10^{-5} \cdot f_{06}$ along all the measuring pressure range and rise above the experimental expanded (k = 2) uncertainty of 250 parts in 10^6 as decreasing the pressure, it was discarded for any following calculation. This is also supported by Figure 3, which shows that the speed of sound values, evaluated from mode (0,6), are not in agreement with the others at the same thermodynamic states. For the remaining modes, the relative dispersion of speed of sound data is lower than 40 parts in 10^6, concluding that the applied acoustic model described above is correct.

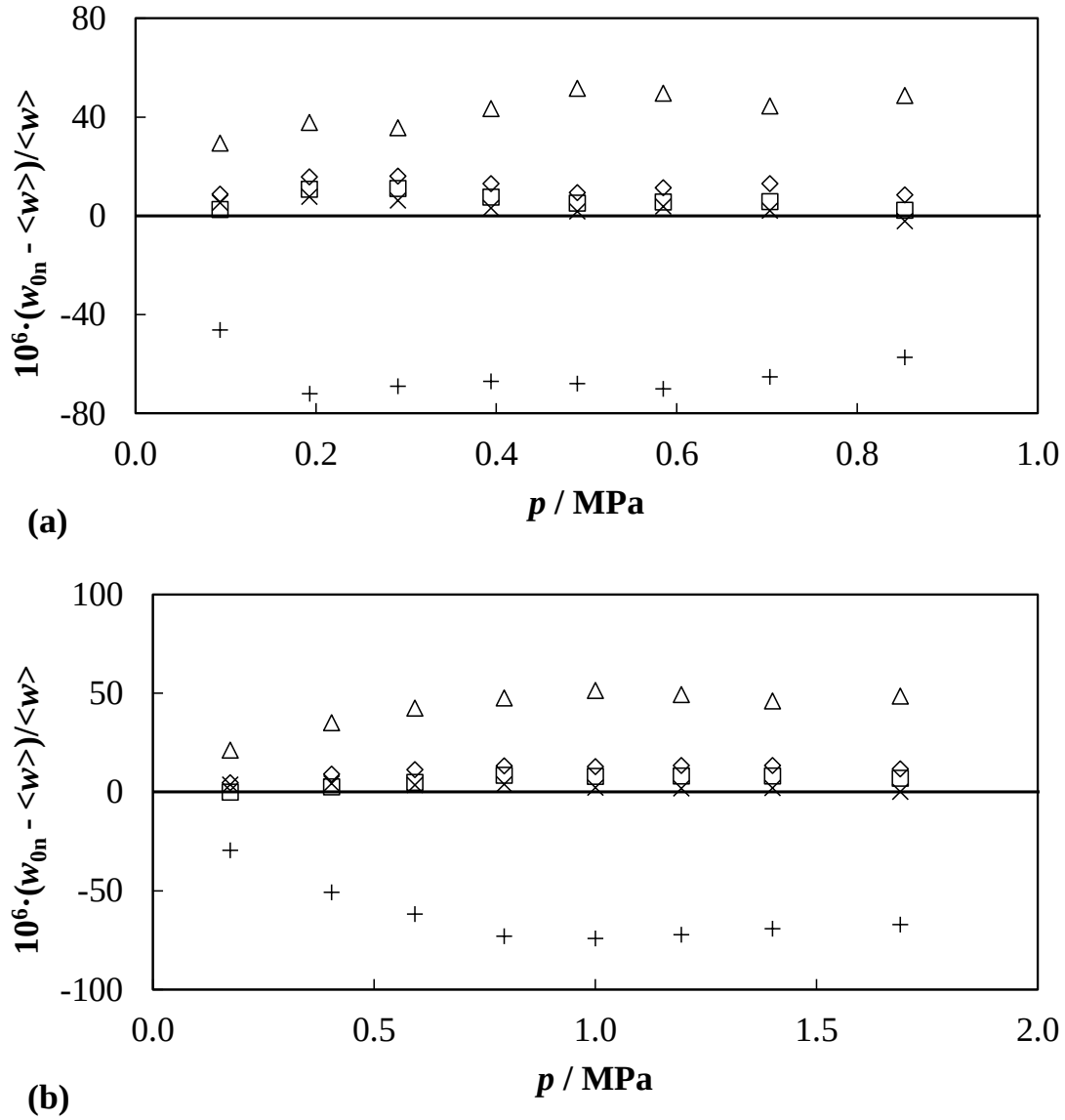

Figure 3. Relative dispersion of the speed of sound $\Delta w = (w_{0n} - \langle w \rangle)/\langle w \rangle$, where $\langle w \rangle$ is the mean value from modes (0,2) to (0,6), as a function of pressure for (a) the mixture (0.60 CO_2 + 0.40 C_3H_8) and (b) the mixture (0.80 CO_2 + 0.20 C_3H_8) at T = 273.16 K and modes △ (0,2), ◇ (0,3), □ (0,4), × (0,5), ＋ (0,6)

A gross estimation of the extent of Δf_{vib} may be made omitting the second term in the square bracket at the right side of Equation (4) and considering an effective vibrational relaxation time τ_{eff} for the mixture. Under this assumption, we obtained vibrational relaxation times at ρ = 1 mol·m^{-3} of τ_{eff} = (1.38 ± 0.13, 1.97 ± 0.18, 1.69 ± 0.15, 1.88 ± 0.13 and 1.79 ± 0.13) μs for the temperatures T = (273.16, 300, 325, 350 and 375) K, respectively. Then, at the point

of greatest value of $\Delta g_{0n}/f_{0n}$, measured for the mixture of higher carbon dioxide content (the relaxing gas) at the highest temperature and highest not neglected resonance mode, the mode (0,5): i) the relative excess halfwidth of mode (0,5) is reduced from (291 to 118) parts in 10^6 after allowing for vibrational relaxation with the τ_{eff} reported, which would involve an increase of experimental expanded (k = 2) uncertainty from (250 to 276) parts in 10^6 as much, and ii) the largest correction to the resonance frequency because of vibrational relaxation is always below 0.5 parts in 10^6. Thus, we are confident that the vibrational relaxation is negligible in the present context.

2.2.2 Cylindrical microwave resonator.

Phase envelope is determined using a cylindrical microwave resonator based on the dielectric constant property change for the phase transition detection which is described in detail in [42], including the set-up of the equipment and the measurements of pure CO_2 in order to check the performance of the technique. A schematic view of the experimental technique is showed in the Fig. 4.

The measure cell consists of a cylindrical resonant cavity, 98.17 cm^3 of volume, with a sapphire tube, 15 cm long, located inside this cavity which contains the sample. The resonant modes of cylindrical cavity depend on the electrical properties of the sample. The cylindrical resonator is made of copper-zirconium (Luvata ZrK015) due to its low conductivity and mechanical simplicity. Two couplings are used to transfer microwave signal, using a vector network analyser (VNA model N5230C) configured to measure the complex scattering coefficient through the cavity and connected to the antennas.

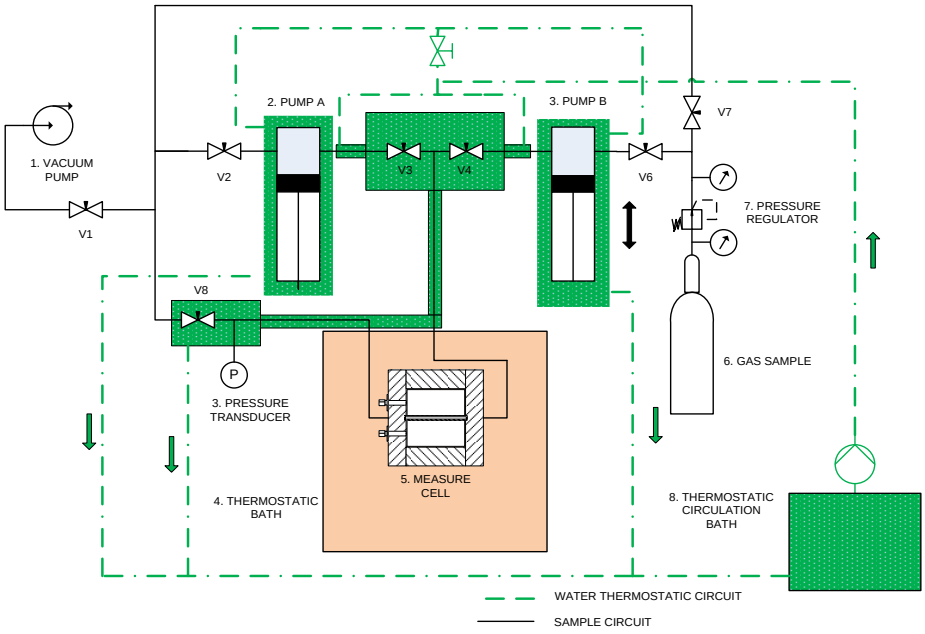

Figure 4. Schematic diagram of the technique for measuring phase envelope [42].

A precision thermostatic bath, which can work in a temperature range from −20°C to 150°C, is used to maintain the measure cell at isothermal conditions. Two syringe pumps A and B operate in a flow rate range from 1 µL/min to 90 mL/min at maximum pressure of 51.7 MPa. Additionally, an external circulation thermostatic bath controls the temperature of syringe pumps and the sample circuit. In order to homogenize the mixture, one of the syringe pumps works with positive displacement and another with negative displacement. A thermometer ASL F100 with two Pt100 sensors was used for measuring temperature and, a Druck DPI-145 pressure indicator with a PDCR 911-1756 external transducer was used for pressure measurements. Both devices were calibrated in our laboratory using equipment traceable to national standards. The corresponding calibration uncertainties are: $U(T)$ = 0.03 K and $U(p)$ = $(4.0 \cdot 10^{-4}\ (p/\mathrm{MPa}) + 0.001)$ MPa with a cover factor k= 2. To estimate the total uncertainty of temperature and pressure, when the bubble point or the dew point is measured, other contributions should be taken into account such as resolution, composition, repeatability and the polynomial adjustment for pressure. resulting in the values $U(T)$ = 0.04 K and $U(p)$ = $(2.2 \cdot 10^{-3}\ (p/\mathrm{MPa}) + 0.001)$ MPa with a cover factor k= 2.

Filling operation is done under homogenous phase conditions. During the isothermal experiment, liquid sample is maintained at constant temperature and the pressure is decreased until the first bubble occurs and, with the reverse procedure, dew point of a gas sample is measured. Phase transition presents a discontinuity in electric permittivity and therefore in resonant modes. The first transversal magnetic mode (TM_{010}) was chosen between the different resonant modes due to its high electric field strength in the axis of the cylindrical cavity, where sample is located, achieving an improvement in sensitivity. Pressure of the sample is controlled by a thermostatic system in the surroundings of the resonant cylindrical cavity. High pressure equilibrium data of fluid mixtures can be measured with this technique which was previously checked measuring phase behavior of pure CO_2 and (CO_2 + CH_4) mixtures [42].

Accurate measurements of resonance frequency are performed by means of a Vector Network Analyser (VNA) from Agilent Technologies, with a frequency range from 300 kHz to 13.5 GHz and a maximum power from 3.98 to 12.59 mW. The VNA instrument measures complex transmission coefficient, S_{21} (ratio of voltage transmitted to incident voltage), which is very important to fit resonance measured data. A model for an ideal resonator is the lumped-element series Resistor Inductor Capacitor (RLC) circuit that was used for the resonant mode TM_{010}. Equation 6 is used for modelling complex transmission coefficient as a function of frequency:

$$|S_{21}(f)| = \frac{\left|\overline{S_{21}}\right|}{\sqrt{1 + 4Q^2\left(\frac{f}{f_0} - 1\right)^2}} \qquad (6)$$

where $|S_{21}(f)|$ is the module of complex transmission coefficient which depends on frequency, $\left|\overline{S_{21}}\right|$ is the maximum value, Q is the quality factor, f is the frequency and f_0 is the resonance frequency. For better fitting results, a variable change was implemented and two

sequential polynomic regressions are performed [43]. Microwave frequency measurements are performed with an uncertainty of 10 ppm which is negligible in comparison with the uncertainty of pressure or temperature measurements.

3. Results.

The 86 speed of sound data were calculated from the average of the repeated acoustic resonance frequencies of the four experimental radial modes (0,2), (0,3), (0,4), and (0,5) using Equation (3), after rejection of mode (0,6) and application of the frequency perturbations of the described acoustic model, at temperatures T = (273.16, 300, 325, 350, and 375) K and pressures p up to 4 MPa for frequencies between (4.1 to 19.8) kHz. The values are reported in Table 2 for mixture (0.60 CO_2 + 0.40 C_3H_8) and Table 3 for mixture (0.80 CO_2 + 0.20 C_3H_8), together with the relative deviations from the AGA8-DC92 EoS [13,14] and GERG-2008 EoS [10,11] evaluated from REFPROP 10 [18].

Table 2. Gas-phase speed of sound $w_{exp}(p,T)$ for the mixture (0.60 CO_2 + 0.40 C_3H_8) with their relative expanded (k = 2) uncertainty(*) and relative deviations $\Delta w_{EoS} = (w_{exp} - w_{EoS})/w_{EoS}$ from the speed of sound predicted by the AGA8-DC92 EoS [13,14] and GERG-2008 EoS [10,11]. The exact mixture compositions with their uncertainties are provided in Table 1. Also, the experimental resonance frequencies f_{0n} after corrections of the acoustic modes used to obtain $w_{exp}(p,T)$ are reported.

p / MPa	w_{exp} / m·s^{-1}	$10^6 \cdot \Delta w_{AGA}$	$10^6 \cdot \Delta w_{GERG}$	f_{02} / Hz	f_{03} / Hz	f_{04} / Hz
			T = 273.16 K			
0.09341	247.590	327	−116	4409.113	7580.203	10699.331
0.19282	245.847	672	−150	4378.086	7526.790	10623.918
0.29079	244.094	1046	−192	4346.866	7473.076	10548.113
0.39417	242.206	1501	−238	4313.233	7415.230	10466.474

0.48965	240.424	1967	−287	4281.500	7360.643	10389.425
0.58477	238.611	2500	−336	4249.184	7305.106	10311.036
0.70301	236.298	3248	−414	4207.966	7234.273	10211.056
0.85292	233.266	4396	−522	4153.950	7141.377	10079.934
			T = 300.00 K			
0.15300	257.606	346	−330	4585.457	7883.318	11127.165
0.36130	254.726	955	−475	4534.178	7795.127	11002.695
0.57462	251.696	1656	−646	4480.217	7702.323	10871.693
0.76434	248.919	2323	−850	4430.771	7617.307	10751.693
0.95467	246.076	3159	−999	4380.153	7530.266	10628.836
1.18105	242.578	4248	−1241	4317.879	7423.187	10477.683
1.38746	239.274	5387	−1502	4259.020	7322.017	10334.872
1.58983	235.922	6695	−1779	4199.338	7219.387	10190.022
1.76559	232.907	8002	−2056	4145.647	7127.093	10059.761
1.97232	229.271	10018	−2220	4080.919	7015.788	9902.633
2.16381	225.792	12393	−2252	4018.964	6909.257	9752.341
			T = 325.00 K			
0.09640	267.973	131	−338	4767.777	8196.817	11569.687
0.28915	265.854	538	−480	4730.077	8131.932	11478.082
0.49033	263.614	1021	−626	4690.194	8063.324	11381.264
0.76321	260.516	1730	−860	4635.028	7968.466	11247.383
0.98537	257.951	2398	−1043	4589.362	7889.954	11136.543
1.19048	255.534	3042	−1254	4546.324	7815.969	11032.082
1.37675	253.303	3681	−1458	4506.602	7747.678	10935.689
1.58771	250.744	4511	−1660	4461.030	7669.329	10825.099
1.79194	248.211	5351	−1908	4415.925	7591.775	10715.655
2.01417	245.417	6422	−2131	4366.201	7506.272	10594.968
2.22719	242.665	7477	−2436	4317.191	7422.020	10476.048

			T = 350.00 K			
0.13989	276.779	141	−382	4922.710	8463.145	11945.596
0.27862	275.548	381	−466	4900.804	8425.461	11892.395
0.48656	273.696	786	−581	4867.823	8368.734	11812.337
0.79055	270.979	1497	−703	4819.451	8285.557	11694.921
1.09466	268.220	2238	−876	4770.334	8201.104	11575.696
1.39409	265.462	3000	−1103	4721.239	8116.690	11456.535
1.68741	262.747	3878	−1280	4672.908	8033.598	11339.272
2.04339	259.395	4971	−1584	4613.226	7930.983	11194.444
			T = 375.00 K			
0.12921	285.753	−35	−457	5080.289	8734.069	12328.004
0.29555	284.546	172	−571	5058.806	8697.096	12275.806
0.48745	283.171	498	−637	5034.331	8654.994	12216.400
0.79036	280.993	1037	−760	4995.552	8588.309	12122.254
0.97695	279.636	1346	−887	4971.396	8546.794	12063.633
1.28414	277.391	1864	−1133	4931.418	8478.047	11966.608
1.58734	275.211	2561	−1247	4892.613	8411.324	11872.440
1.78169	273.795	2967	−1389	4867.400	8367.962	11811.236

(*) Expanded uncertainties (k = 2): $U(p)$ = (2.2 to 3.8)·10^{-4} MPa; $U(T)$ = 5 mK; $U_r(w)$ = 2.5·10^{-4} m·s^{-1}/ m·s^{-1}.

Table 3. Gas-phase speed of sound $w_{exp}(p,T)$ for the (0.80 CO_2 + 0.20 C_3H_8) mixture with their relative expanded (k = 2) uncertainty(*) and relative deviations $\Delta w_{EoS} = (w_{exp} - w_{EoS})/w_{EoS}$ from the speed of sound predicted by the AGA8-DC92 EoS [13,14] and GERG-2008 EoS [10,11]. The exact mixture compositions with their uncertainties are provided in Table 1. Also, the experimental resonance frequencies f_{0n} after corrections of the acoustic modes used to obtain $w_{exp}(p,T)$ are reported.

p / MPa	w_{exp} / m·s^{-1}	$10^6 \cdot \Delta w_{AGA}$	$10^6 \cdot \Delta w_{GERG}$	f_{02} / Hz	f_{03} / Hz	f_{04} / Hz
			T = 273.16 K			
0.17442	251.019	363	2	4470.188	7685.166	10847.475
0.40428	247.963	932	73	4415.718	7591.512	10715.295
0.59194	245.387	1514	130	4369.805	7512.599	10603.909
0.79421	242.523	2302	203	4318.791	7424.817	10480.006
1.00052	239.495	3301	279	4264.866	7332.021	10349.036
1.19464	236.536	4476	353	4212.127	7241.381	10221.087
1.40066	233.265	6042	441	4153.825	7141.200	10079.661
1.68967	228.411	9003	585	4067.358	6992.489	9869.768
			T = 300.00 K			
0.15849	262.372	297	−67	4670.284	8029.171	11333.024
0.47740	259.135	915	−46	4612.638	7929.994	11193.059
0.96014	254.060	2047	−27	4522.271	7774.570	10973.679
1.46891	248.450	3546	−28	4422.346	7602.783	10731.182
1.98784	242.410	5538	−25	4314.769	7417.833	10470.149
2.51536	235.876	8241	2	4198.399	7217.803	10187.786
3.02555	229.073	11807	5	4077.225	7009.422	9893.877
3.23569	226.126	13791	105	4024.814	6919.284	9766.266
			T = 325.00 K			
0.11563	272.540	202	−90	4849.031	8336.489	11766.834
0.48496	269.585	746	−109	4796.427	8245.980	11639.070
0.99139	265.455	1622	−146	4722.856	8119.471	11460.494
1.48068	261.370	2608	−206	4650.086	7994.353	11283.901
1.98719	257.041	3796	−278	4573.001	7861.788	11096.776
2.52348	252.338	5247	−372	4489.244	7717.774	10893.490
2.98097	248.225	6659	−464	4415.993	7591.821	10715.720
3.36390	244.709	7987	−550	4353.399	7484.193	10563.793

			T = 350.00 K			
0.13074	281.726	35	−251	5010.686	8614.397	12159.099
0.49094	279.431	455	−278	4969.823	8544.082	12059.839
0.97289	276.333	1051	−362	4914.653	8449.224	11925.936
1.47521	273.092	1794	−435	4856.922	8349.947	11785.829
1.96912	269.877	2563	−561	4799.653	8251.481	11646.845
2.51998	266.292	3577	−656	4735.802	8141.689	11491.887
3.00725	263.099	4494	−807	4678.924	8043.888	11353.840
3.36826	260.751	5282	−859	4637.100	7971.996	11252.356
			T = 375.00 K			
0.12954	290.698	−96	−339	5168.194	8885.198	12541.332
0.47413	288.928	173	−410	5136.681	8830.952	12464.752
0.99076	286.300	682	−481	5089.874	8750.470	12351.131
1.49136	283.761	1203	−592	5044.629	8672.669	12241.338
2.00136	281.202	1810	−690	4999.026	8594.258	12130.672
2.49622	278.742	2442	−801	4955.188	8518.882	12024.302
2.99485	276.307	3162	−874	4911.809	8444.295	11919.023
3.76978	272.569	4215	−1124	4845.198	8329.784	11757.369

(*) Expanded uncertainties (k = 2): $U(p)$ = (2.2 to 3.8)·10^{-4} MPa; $U(T)$ = 5 mK; $U_r(w)$ = 2.5·10^{-4} m·s^{-1}/ m·s^{-1}.

The uncertainty budget for the speed of sound is listed in Table 4. The average of the expanded (k = 2) relative uncertainty of all the speed of sound datasets leads to the overall expanded (k = 2) uncertainty $U_r(w)$ = 250 parts in 10^6 (0.025 %). The procedure for the evaluation of each uncorrelated component of the uncertainty follows from the application of the Expression of Uncertainty in Measurement (GUM) [44,45] and was explained in other works [22,31]. The main contribution is due to the uncertainty of the speed of sound in argon, which amounts up to $u_r(Ar_{EoS})$ = 100 parts in 10^6 (0.01 %), and has to be introduced in the dimensional

characterization of the internal radius of the resonance cavity by acoustic measurements. The second contribution comes from the certified uncertainty of the gas composition, which results in a contribution of u_r = 70 parts in 10^6 to all the measurements.

Table 4. Uncertainty budget for the speed of sound measurements w_{exp}. Unless otherwise specified, uncertainties are indicated with a coverage factor k = 1.

Source		Magnitude	Contribution to the speed of sound uncertainty, $10^6 \cdot u_r(w_{exp})$
Temperature	Calibration	0.002 K	
	Resolution	$7.2 \cdot 10^{-7}$ K	
	Repeatability	$3.5 \cdot 10^{-5}$ K	
	Gradient (across hemispheres)	$1.1 \cdot 10^{-3}$ K	
	Sum	0.0025 K	5.0
Pressure	Calibration	$(3.75 \cdot 10^{-5} \cdot (p/\text{MPa}) + 1 \cdot 10^{-4})$ MPa	
	Resolution	$2.9 \cdot 10^{-5}$ MPa	
	Repeatability	$3.7 \cdot 10^{-6}$ MPa	
	Sum	$(1.1 \text{ to } 1.9) \cdot 10^{-4}$ MPa	6.4
Gas composition	Purity	$1.4 \cdot 10^{-6}$ kg/mol	
	Molar mass	$6.0 \cdot 10^{-6}$ kg/mol	
	Sum	$6.2 \cdot 10^{-6}$ kg/mol	73
Radius from speed of sound in Ar	Temperature	$1.5 \cdot 10^{-9}$ m	
	Pressure	$1.6 \cdot 10^{-10}$ m	
	Gas Composition	$4.1 \cdot 10^{-9}$ m	
	Frequency fitting	$4.9 \cdot 10^{-7}$ m	
	Regression	$1.7 \cdot 10^{-6}$ m	
	Equation of State	$2.3 \cdot 10^{-6}$ m	
	Dispersion of modes	$2.9 \cdot 10^{-6}$ m	
	Sum	$4.2 \cdot 10^{-6}$ m	98
Frequency fitting		0.010 Hz	1.7
Dispersion of modes		$3.0 \cdot 10^{-3}$ m·s^{-1}	12
Sum of all contributions to w_{exp}			125
$10^6 \cdot U_r(w_{exp})$ (k = 2)			250

Concerning determination of phase envelope, the (0.60 CO_2 + 0.40 C_3H_8) mixture was measured in the temperature range from 229.15 K to 329.60 K and in the pressure range from 0.2 MPa to 6.8 MPa, including the retrograde zone considering the critical reference point calculated with the GERG 2008 [10,11], using the software REFPROP [18] whereas the range of measurements for the (0.80 CO_2 + 0.20 C_3H_8) mixture was from 233.15 K to 310.36 K in temperature, and from 0.4 MPa to 6.7 MPa in pressure. Table 5 and Table 6 contain the experimental data and their comparison with the calculated pressure using GERG-2008 EoS. In addition, pressure and temperature uncertainties for these data were calculated taking into account the calibration and the repeatability of the measurements, obtaining the values given at the bottom of the tables.

Table 5**.** Phase equilibria data[a] for the (0.60 CO_2 + 0.40 C_3H_8) mixture and comparison with data calculated using the GERG-2008 EoS [11]. The exact mixture compositions with their uncertainties are provided in Table 1.

T_{exp} / K	Set-up	p_{exp} / MPa	p_{GERG} / MPa	Δp / %[b]	Set-up	p_{exp} / MPa	p_{GERG} / MPa	Δp / %[b]
229.37	Bubble	0.738	0.738	−0.10	Dew	0.227	0.226	−0.08
233.35	Bubble	0.845	0.848	0.36	Dew	0.272	0.270	−0.67
238.36	Bubble	1.005	1.002	−0.33	Dew	0.334	0.334	0.02
243.35	Bubble	1.180	1.175	−0.46	Dew	0.411	0.409	−0.58
248.34	Bubble	1.358	1.367	0.68	Dew	0.496	0.496	−0.07
253.35	Bubble	1.594	1.581	−0.85	Dew	0.595	0.598	0.60
258.34	Bubble	1.825	1.815	−0.56	Dew	0.717	0.715	−0.19
263.34	Bubble	2.070	2.073	0.13	Dew	0.846	0.850	0.54
268.34	Bubble	2.337	2.353	0.67	Dew	1.004	1.005	0.05
273.34	Bubble	2.640	2.657	0.62	Dew	1.176	1.181	0.44
278.33	Bubble	2.982	2.984	0.07	Dew	1.388	1.381	−0.53
283.38	Bubble	3.342	3.339	−0.08	Dew	1.599	1.610	0.68

288.40	Bubble	3.711	3.716	0.15	Dew	1.870	1.868	−0.13
293.41	Bubble	4.128	4.116	−0.28	Dew	2.158	2.159	0.04
298.22	Bubble	4.539	4.521	−0.4	Dew	2.476	2.475	−0.05
303.36	Bubble	4.966	4.972	0.12	Dew	2.867	2.858	−0.33
308.46	Bubble	5.439	5.435	−0.09	Dew	3.294	3.292	−0.05
313.47	Bubble	5.915	5.893	−0.37	Dew	3.783	3.784	0.02
318.49	Bubble	6.329	6.338	0.14	Dew	4.359	4.362	0.06
323.49	Bubble	6.721	6.719	−0.03	Dew	5.068	5.063	−0.10
324.49	Bubble	6.773	6.778	0.08	Dew	5.223	5.227	0.08
325.49	Bubble	6.822	6.827	0.07	Dew	5.394	5.402	0.14
326.47	Bubble	6.859	6.861	0.03	Dew	5.579	5.589	0.18
327.44	Bubble	6.874	6.873	0.01	Dew	5.807	5.794	−0.23
328.41	Dew[c]	6.857	6.861	0.06	Dew	6.043	6.034	−0.14
328.53	Dew[c]	6.865	6.856	−0.14	Dew	6.056	6.068	0.19
328.73	Dew[c]	6.844	6.844	0.00	Dew	6.111	6.127	0.26
328.93	Dew[c]	6.834	6.827	−0.1	Dew	6.201	6.192	−0.14
329.53	Dew[c]	6.724	6.702	−0.32	Dew	6.459	6.459	0.01
329.60	Dew[c]	6.681	6.655	−0.39	Dew	6.538	6.524	−0.22

[a] Expanded uncertainty (k = 2): $U(T)$ = 0.04 K; $U(p)$ = (2.2·10^{-3} (p/MPa) + 0.001) MPa.

[b] δp / % = 100·(p_{exp}/p_{calc} − 1).

[c] Retrograde dew point

Table 6. Phase equilibria data[a] for the (0.80 CO_2 + 0.20 C_3H_8) mixture and comparison with data calculated using the GERG-2008 EoS [11]. The exact mixture compositions with their uncertainties are provided in Table 1.

T_{exp} / K	Set-up	p_{exp} / MPa	p_{GERG} / MPa	Δp / %[b]	Set-up	p_{exp} / MPa	p_{GERG} / MPa	Δp / %[b]
233.36	Bubble	0.923	0.921	0.17	Dew	0.497	0.495	0.40
238.37	Bubble	1.095	1.098	−0.27	Dew	0.609	0.612	−0.49
243.36	Bubble	1.296	1.297	−0.08	Dew	0.748	0.748	0.00

248.35	Bubble	1.522	1.521	0.07	Dew	0.903	0.908	−0.55
253.36	Bubble	1.775	1.772	0.16	Dew	1.090	1.094	−0.37
258.35	Bubble	2.056	2.050	0.28	Dew	1.305	1.308	−0.23
263.35	Bubble	2.362	2.359	0.15	Dew	1.545	1.555	−0.67
268.34	Bubble	2.707	2.697	0.36	Dew	1.839	1.838	0.05
273.32	Bubble	3.072	3.068	0.14	Dew	2.162	2.159	0.14
278.34	Bubble	3.478	3.475	0.08	Dew	2.526	2.527	−0.04
283.33	Bubble	3.911	3.916	−0.12	Dew	2.954	2.942	0.41
288.33	Bubble	4.409	4.393	0.36	Dew	3.411	3.412	−0.03
293.34	Bubble	4.921	4.908	0.26	Dew	3.916	3.945	−0.74
298.33	Bubble	5.471	5.456	0.27	Dew	4.544	4.547	−0.07
303.34	Bubble	6.038	6.035	0.05	Dew	5.265	5.241	0.46
308.34	Bubble	6.614	6.602	0.19	Dew	6.073	6.074	−0.02
308.54	Bubble	6.632	6.622	0.15	Dew	6.117	6.113	0.07
308.95	Bubble	6.684	6.662	0.33	Dew	6.195	6.194	0.01
309.16	Bubble	6.695	6.681	0.21	Dew	6.244	6.237	0.11
309.35	Bubble	6.714	6.697	0.25	Dew	6.285	6.277	0.12
309.55	Bubble	6.726	6.713	0.19	Dew	6.328	6.320	0.12
309.96	Bubble	6.746	6.741	0.08	Dew	6.420	6.414	0.09
310.16	Bubble	6.747	6.751	−0.06	Dew	6.451	6.463	−0.19
310.36	Bubble	6.772	6.759	0.19	Dew	6.51	6.516	−0.09

[a] Expanded uncertainty (k = 2): $U(T)$ = 0.04 K; $U(p)$ = ($2.2 \cdot 10^{-3}$ (p/MPa) + 0.001) MPa.

[b] δp / % = $100 \cdot (p_{exp}/p_{calc} - 1)$.

4. Discussion.

4.1 Speed of sound.

Relative deviations of the experimental speed of sound data from the calculated values by AGA8-DC92 EoS [13,14] and GERG-2008 EoS [10,11] are listed in Table 2 and Table 3 (in the former section), and also depicted in Figure 5 and Figure 6.

Nearly all the differences, when comparing to the GERG-2008 EoS [10,11], remain outside $U_r(w_{exp})$ = 250 parts in 10^6 (0.025 %), with the exceptions of the deviations at the isotherm of 300 K along all pressures and the isotherms of 273.16 K and 325 K up to intermediate pressures for the (0.80 CO_2 + 0.20 C_3H_8) mixture and the state points limited to the lower pressure range for all the temperatures and both mixtures, which approach to zero while decreasing pressure. This good agreement with the values close to zero pressure is a good indicator of the stability of the mixture composition during the measuring process, so we conclude that the measurements are not affected by the absorption and desorption of the gas with the cavity wall material, condensation during the gas filling procedure or stratification of the mixtures within the sampling gas bottles.

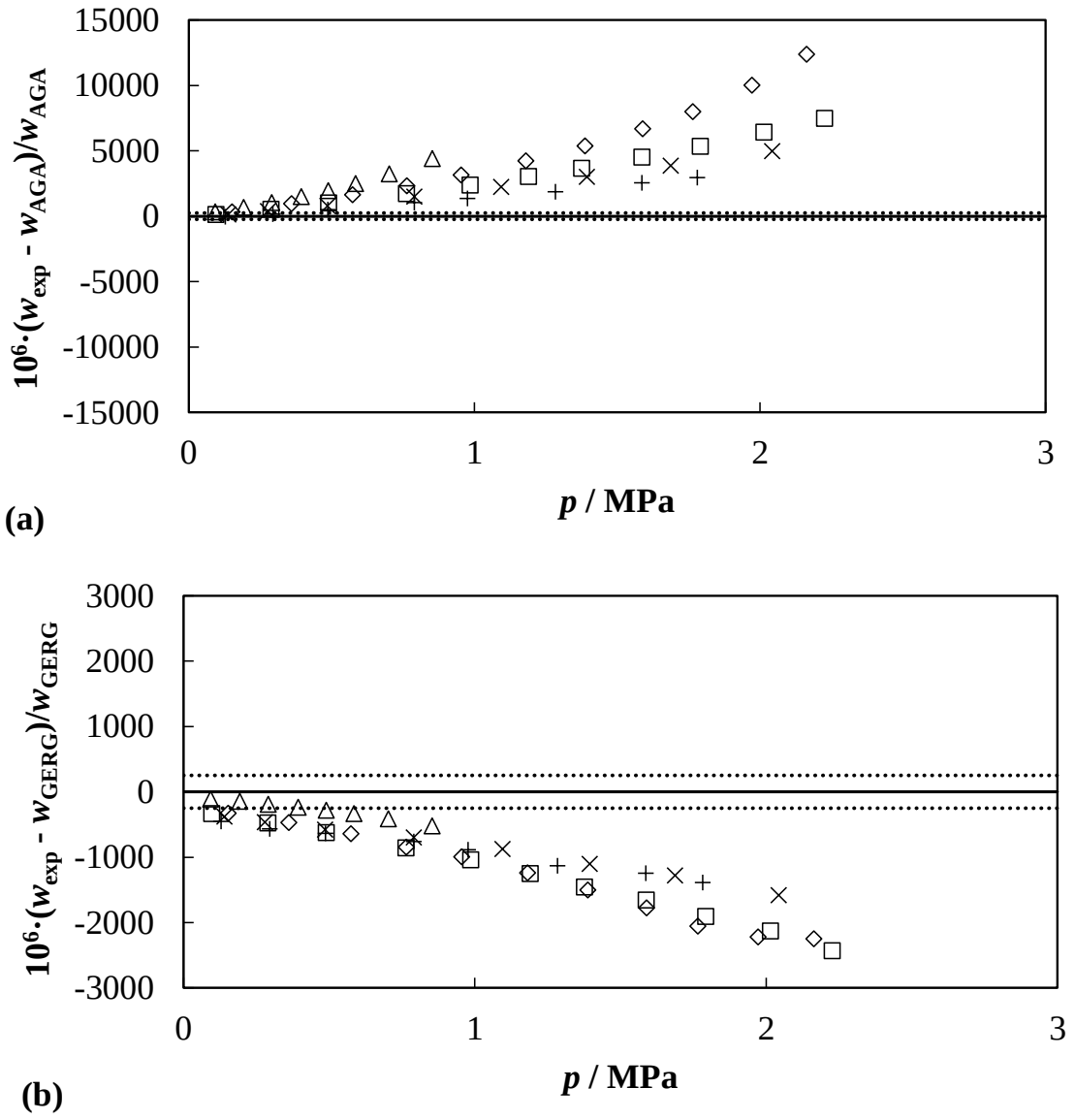

Figure 5. Relative deviations of experimental speed of sound from speed of sound values calculated from (a) AGA8-DC92 EoS [13,14] and (b) GERG-2008 EoS [10,11] as function of pressure for the (0.60 CO_2 + 0.40 C_3H_8) mixture at temperatures T = Δ 273.16 K, ◇ 300 K, □ 325 K, × 350 K, + 375 K. Dotted line depicts the expanded (k = 2) uncertainty of the experimental speed of sound.

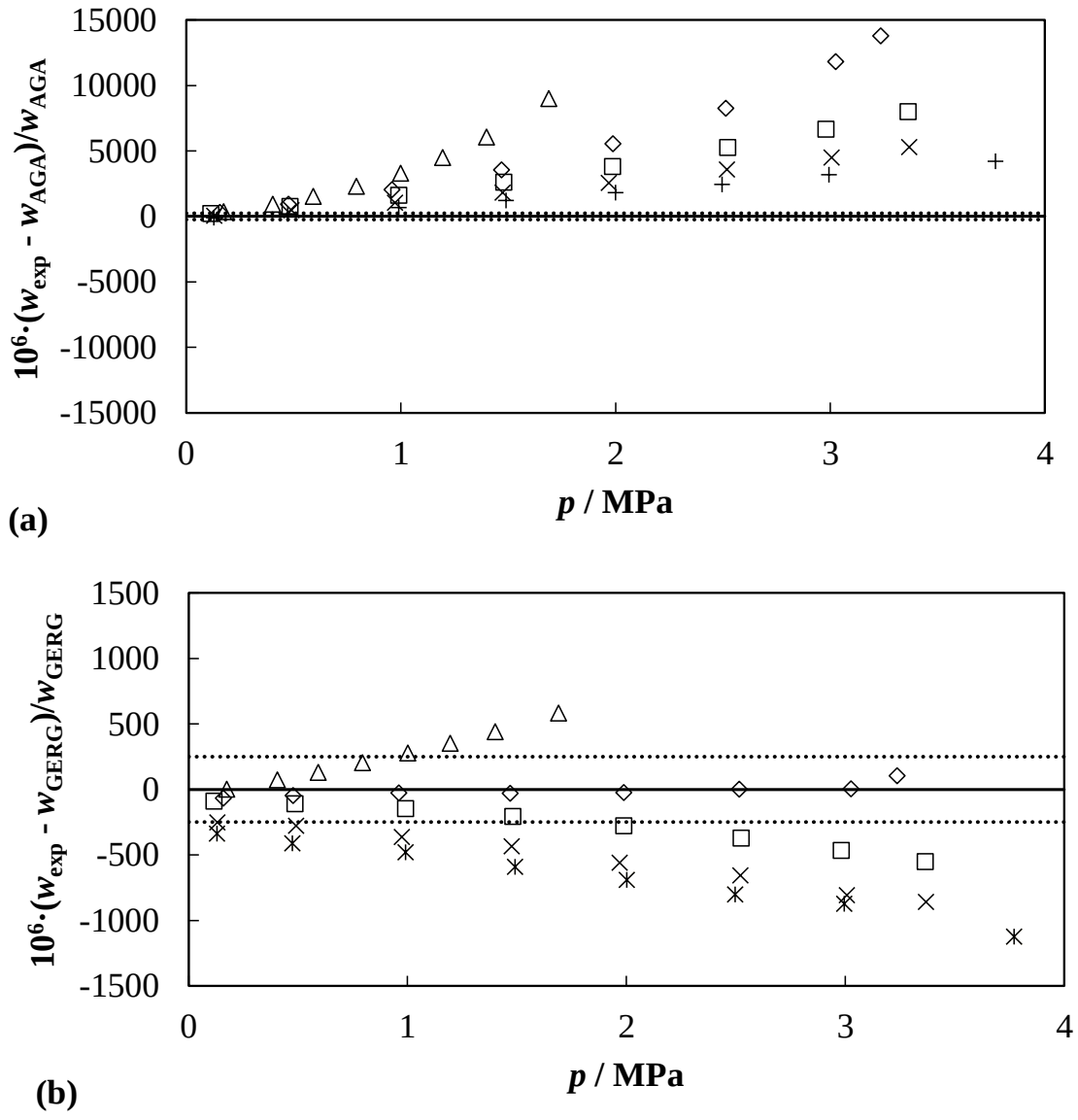

Figure 6. Relative deviations of experimental speed of sound from speed of sound values calculated from (a) AGA8-DC92 EoS [13,14] and (b) GERG-2008 EoS [10,11] as function of pressure for the (0.80 CO_2 + 0.20 C_3H_8) mixture at temperatures T = Δ 273.16 K, ◇ 300 K, □ 325 K, × 350 K, + 375 K. Dotted line depicts the expanded (k = 2) uncertainty of the experimental speed of sound.

However, discrepancies are well explained within the declared expanded (k = 2) uncertainty of the GERG-2008 EoS [10,11] in speed of sound $U_r(w_{GERG})$ = 10000 parts in 10^6 (1.0 %) for

binary mixtures with no departure function and only adjusted reducing function. Though the AGA8-DC92 EoS [13,14] does not report any uncertainty for this kind of mixtures, even assuming the same model uncertainty than the GERG-2008 EoS [10,11], deviations are also within these limits.

Deviations increase with increasing pressure, with systematic negative trends with respect to GERG-2008 EoS [10,11] that decrease with decreasing x_{C3H8}, in contrast to positive differences according to AGA8-DC92 EoS [13,14] that increase with decreasing x_{C3H8}. Average absolute deviations $\Delta_{AAD} = \left[N^{-1}\sum_{i=1}^{N}\left|\left(w_{exp} - w_{EoS}\right)/w_{EoS}\right|_i\right]$ between experimental and calculated values are better than 0.093 % for the (0.60 CO_2 + 0.40 C_3H_8) mixture and less than 0.035 % for the (0.80 CO_2 + 0.20 C_3H_8) mixture with respect to the GERG-2008 EoS [10,11]. The corresponding Δ_{AAD} using AGA8-DC92 EoS [13,14] are (0.27 and 0.34) %, respectively. These results are consistent with the declared uncertainty of the two equations.

Each squared speed of sound data set $w^2(p_i,T)$ at several pressures p_i and reference to the same temperature T were analyzed by fitting to a polynomial function of the pressure:

$$w^2\left(p,T\right) = A_0\left(T\right) + A_1\left(T\right)p + A_2\left(T\right)p^2 + A_3\left(T\right)p^3 \qquad (7)$$

with the adjustable parameters A_i listed in Table 7 together with their expanded (k = 2) uncertainty $U(A_i)$ computed by the Monte Carlo method [47].

Table 7. Fitting parameters $A_i(T)$ of Eq. (7) with their corresponding expanded (k = 2) uncertainties, determined by the Monte Carlo method, and the root mean square (Δ_{RMS}) of the residuals of the fitting.

T / K	$A_0(T)$ / $m^2 \cdot s^{-2}$	$10^5 \cdot A_1(T)$ / $m^2 \cdot s^{-2} \cdot Pa^{-1}$	$10^{12} \cdot A_2(T)$ / $m^2 \cdot s^{-2} \cdot Pa^{-2}$	$10^{18} \cdot A_3(T)$ / $m^2 \cdot s^{-2} \cdot Pa^{-3}$	Δ_{RMS} of residuals / ppm
		(0.60 CO_2 + 0.40 C_3H_8)			
273.16	62092 ± 13	−842.9 ± 6.4	−671 ± 65		18

300.00	67426 ± 16	−693.2 ± 5.6	−258 ± 54	−24 ± 15	40
325.00	72368 ± 10	−580.9 ± 2.0	−108.8 ± 8.1		20
350.00	77287 ± 15	−487.4 ± 3.3	−10 ± 15		19
375.00	82186 ± 18	−412.4 ± 4.5	39 ± 23		35
			(0.80 CO_2 + 0.20 C_3H_8)		
273.16	64152 ± 17	−650.2 ± 7.4	−200 ± 89	−88 ± 31	7
300.00	69675 ± 14	−525.2 ± 3.7	−73 ± 25	−23.2 ± 4.8	25
325.00	74777 ± 11	−431.5 ± 1.4	−33.4 ± 3.9		3
350.00	79846 ± 12	−361.4 ± 1.6	27.4 ± 4.4		37
375.00	84899 ± 13	−301.8 ± 1.6	54.3 ± 3.9		27

A second order polynomial was required for most of the isotherms, except for T = 273.16 K for the mixture (0.60 CO_2 + 0.40 C_3H_8) and T = (273.16 and 300) K for the mixture (0.80 CO_2 + 0.20 C_3H_8), in order to meet the criteria of residuals within the experimental uncertainty, random distribution of the residuals when represented versus the pressure (independent variable) and versus the experimental speed of sound (dependent variable), and statistical significance of the regression parameters as given by the *p*-test. The estimated uncertainties of each speed of sound value are used as weights in this regression. Relative residuals of the fitting are plotted in Figure 7 for the two mixtures, with a root mean square Δ_{RMS} less than 30 parts in 10^6 in all the cases.

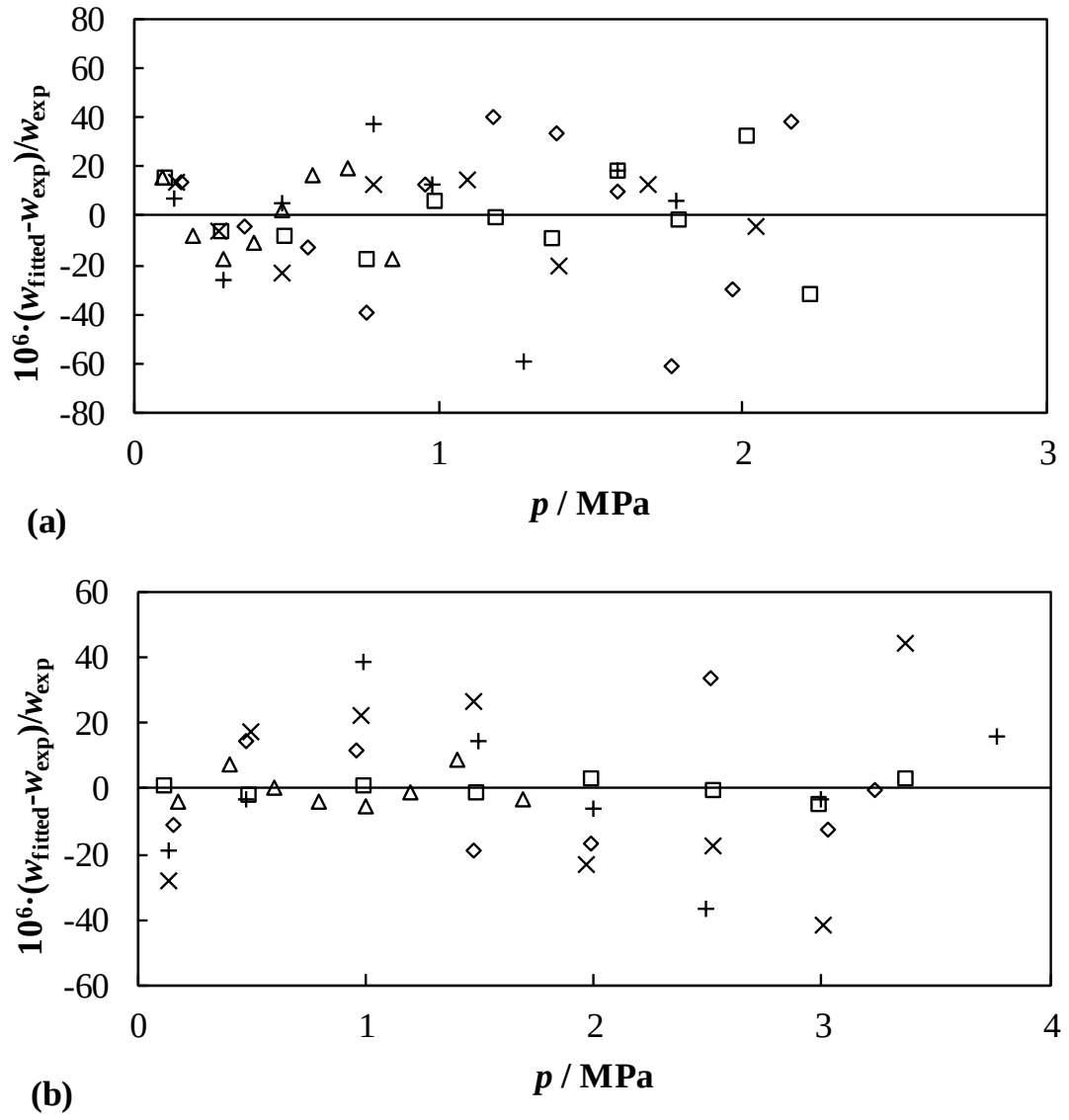

Figure 7. Speed of sound residuals from Eq. (7) as a function of the pressure for (a) the (0.60 CO_2 + 0.40 C_3H_8) mixture and (b) the (0.80 CO_2 + 0.20 C_3H_8) mixture at temperatures T = △ 273.16 K, ◇ 300 K, □ 325 K, × 350 K, ＋ 375 K.

4.2 Perfect-gas heat capacities.

Molar perfect-gas heat capacities at constant pressure $C_{p,m}^{pg}$ are obtained from the fitting parameters $A_0(T)$ of Table 7 by:

$$\gamma^{pg} = \frac{C_{p,m}^{pg}}{C_{V,m}^{pg}} = \frac{C_{p,m}^{pg}}{C_{p,m}^{pg} - R} = \frac{M}{RT} A_0 \quad (8)$$

where γ^{pg} is the heat capacity ratio as perfect-gas "*pg*" (zero pressure), M is the molar mass of the mixture (Table 1) and R is the exact value of the molar gas constant [46]. Table 8 reports the experimental results γ^{pg} and $C_{p,m}^{pg}$ together with their expanded (k = 2) uncertainty $U(\gamma^{pg})$ and $U(C_{p,m}^{pg})$, which is better than 0.31 % for the (0.60 CO_2 + 0.40 C_3H_8) mixture and less than 0.17 % for the (0.80 CO_2 + 0.20 C_3H_8) mixture, and the comparison with the two reference EoS. This uncertainty includes the contributions of temperature, molar mass, and fitted A_0.

Table 8. Adiabatic coefficient γ^{pg}, isobaric heat capacity $C_{p,m}^{pg}$, acoustic second virial coefficient β_a, and acoustic third virial coefficient γ_a for the (CO_2 + C_3H_8) mixtures determined in this work, with their corresponding relative expanded (k = 2) uncertainty, and comparison with AGA8-DC92 and GERG-2008 EoS. The superscript *pg* indicates perfect-gas property.

T / K	γ^{pg}	$10^2 \cdot U_r(\gamma^{pg})$	$10^2 \cdot \Delta\gamma^{pg}_{AGA^{(*)}}$	$10^2 \cdot \Delta\gamma^{pg}_{GERG^{(*)}}$	$C_{p,m}^{pg}$ / J·mol^{-1}·K^{-1}	$10^2 \cdot U_r(C_{p,m}^{pg})$	$10^2 \cdot \Delta C^{pg}_{p,m\,AGA^{(*)}}$	$10^2 \cdot \Delta C^{pg}_{p,m\,GERG^{(*)}}$
(0.60 CO_2 + 0.40 C_3H_8)								
273.16	1.20412	0.042	−0.0066	−0.029	49.047	0.25	0.032	0.14
300.00	1.19058	0.044	−0.021	−0.055	51.943	0.27	0.11	0.29
325.00	1.17955	0.039	−0.019	−0.060	54.621	0.26	0.11	0.33
350.00	1.16974	0.041	−0.025	−0.066	57.298	0.29	0.15	0.39
375.00	1.16097	0.043	−0.043	−0.080	59.968	0.31	0.27	0.49
(0.80 CO_2 + 0.20 C_3H_8)								
273.16	1.24359	0.034	0.011	−0.0012	42.448	0.17	−0.047	0.0042
300.00	1.22982	0.028	0.014	−0.0068	44.493	0.15	−0.057	0.029
325.00	1.21834	0.025	0.0082	−0.018	46.394	0.14	−0.035	0.081
350.00	1.20801	0.025	−0.010	−0.038	48.286	0.15	0.052	0.18
375.00	1.19882	0.025	−0.032	−0.056	50.134	0.15	0.16	0.28
	$10^7 \cdot \beta_a$ / m^3·mol^{-1}	$10^2 \cdot U_r(\beta_a)$	$10^2 \cdot \Delta\beta_{a,AGA^{(*)}}$	$10^2 \cdot \Delta\beta_{a,GERG^{(*)}}$	$10^{10} \cdot \gamma_a$ / (m^3·mol^{-1})^2	$10^2 \cdot U_r(\gamma_a)$	$10^2 \cdot \Delta\gamma_{a,AGA^{(*)}}$	$10^2 \cdot \Delta\gamma_{a,GERG^{(*)}}$
(0.60 CO_2 + 0.40 C_3H_8)								

273.16	−3083	0.78	−5.0	−0.44	155	35	−40	−51
300.00	−2564	0.78	−5.1	0.74	243	21	−12	−15
325.00	−2169.2	0.34	−5.0	1.3	229.7	3.6	−7.1	−11
350.00	−1835.1	0.69	−5.2	1.4	231.4	7.1	5.4	−2.1
375.00	−1564.6	1.1	−4.9	2.0	222	12	13	2.6
				(0.80 CO_2 + 0.20 C_3H_8)				
273.16	−2302	1.1	−2.9	−0.019	263	27	79	28
300.00	−1880.3	0.70	−3.7	0.36	215	10	26	15
325.00	−1559.4	0.33	−4.4	−0.0071	160.7	2.4	3.2	−6.0
350.00	−1317.1	0.46	−3.7	1.0	166.3	2.8	19	6.2
375.00	−1108.5	0.52	−3.2	1.7	159.8	2.9	25	12

(*) $\Delta X_{\mathrm{EoS}} = (X_{\mathrm{exp}} - X_{\mathrm{EoS}})/X_{\mathrm{EoS}}$ with $X = \gamma^{\mathrm{pg}}$, $C_{\mathrm{p,m}}^{\mathrm{pg}}$, β_{a}, γ_{a}; and EoS = AGA8-DC92 [13,14], GERG-2008 [10,11].

Perfect-gas heat capacities for the (CO_2 + C_3H_8) mixture evaluated from the models are obtained from the spectroscopy data of the unpublished work of Chao et al. [47] for pure carbon dioxide with an expanded (k = 2) uncertainty of 0.02 %, and the perfect-gas heat capacity from the spectroscopy data of Chao et al. [48] for pure propane with an expanded (k = 2) uncertainty between (0.3 to 0.5) %, which slightly differ from the speed of sound data of Trusler et al. [35] used in the development of the current reference EoS for pure propane [49]. Thus, the estimated expanded (k = 2) uncertainty of $C_{\mathrm{p,m}}^{\mathrm{pg}}$ from the two models is by about 0.2 % for the (0.60 CO_2 + 0.40 C_3H_8) mixture and 0.1 % for the (0.80 CO_2 + 0.20 C_3H_8) mixture. As shown in Table 8, the relative deviations of the experimental $C_{\mathrm{p,m}}^{\mathrm{pg}}$ from the calculated values by AGA8-DC92 EoS [13,14] are half of the relative deviations with respect to GERG-2008 EoS [10,11] and within the model expanded (k = 2) uncertainties. Average absolute relative deviations

are Δ_{AAD} (AGA) = 0.10 % and Δ_{AAD} (GERG) = 0.22 %.

$C_{p,m}^{pg}$ results are fitted to Planck-Einstein-like functions as those derived from statistical mechanics for the shape of the heat capacity as function of the temperature:

$$\frac{C_{p,m}^{pg}}{R} = v_0 + v_1 \frac{\left(u_1/T\right)^2 e^{u_1/T}}{\left(e^{u_1/T} - 1\right)^2} \tag{9}$$

with v_0 = 4.856 ± 0.049, v_1 = 6.91 ± 0.14, and u_1 = 1420 ± 28 K for the (0.60 CO_2 + 0.40 C_3H_8) mixture and v_0 = 4.349 ± 0.021, v_1 = 4.818 ± 0.051, and u_1 = 1402 ± 16 K for the (0.80 CO_2 + 0.20 C_3H_8) mixture, where the terms are empirical coefficients. The estimated expanded (k = 2) experimental uncertainties $U(C_{p,m}^{pg})$ where used as weights in the regression, with root mean squares of the residuals Δ_{RMS} equal to 0.043 % and 0.020 %, within the average $U(C_{p,m}^{pg})$ = 0.28 % and 0.15 % for the (0.60 CO_2 + 0.40 C_3H_8) and (0.80 CO_2 + 0.20 C_3H_8) mixtures, respectively.

4.3 Virial coefficients.

Second acoustic virial coefficient β_a is obtained, for each isotherm, from A_0 and A_1 of Table 7 by:

$$\beta_a = \frac{M}{\gamma^{pg}} A_1 = RT \frac{A_1}{A_0} \tag{10}$$

whereas, third acoustic virial coefficient γ_a is derived, at each temperature, from A_0, A_1, and A_2 fitted parameters of Table 7:

$$\gamma_a = \frac{RTM}{\gamma^{pg}} A_2 + B\beta_a = \frac{RT}{A_0}\left(RTA_2 + BA_1\right) \tag{11}$$

where B is second density virial coefficient of the mixture for each isotherm. Table 8 lists the results of β_a and γ_a, together with their relative expanded (k = 2) uncertainty $U(\beta_a)$ between (0.33 to 1.1) % and $U(\gamma_a)$ ranging from (2.4 to 35) %, and the comparison with the predicted values using the AGA8-DC92 EoS [13,14] and GERG-2008 EoS [10,11]. Relative deviations

of β_a from EoS could only be explained within the uncertainty for the GERG-2008 EoS [10,11], in particular, at the intermediate isotherms of mixture (0.80 CO_2 + 0.20 C_3H_8); Δ_{AAD} (GERG) = 0.89 %, for the two mixtures, is slightly larger than the average $U(\beta_a)$ = 0.68 %. In contrast, discrepancies with the AGA8-DC92 [13,14] are always negative and around six times the mean $U(\beta_a)$, with a Δ_{AAD} (AGA) = 4.3 %. For γ_a, there is no good agreement with any of the two studied models, with Δ_{AAD} (GERG) = 15 % and Δ_{AAD} (AGA) = 23 % in comparison with the mean $U(\gamma_a)$ = 12 % although our results are more in line with the predicted values using GERG-2008 EoS [10,11]. The relative differences tend to decrease with increasing temperature, but with no clear trend with composition. This behavior for the two acoustic virial coefficients is expected since, as discussed above with regard to speed of sound data, the overall relative deviations are lower for the higher isotherms and more consistent with the GERG-2008 model [10,11] than the AGA8-DC92 model [13,14].

For further validation of our speed of sound data, second density virial coefficients B of the (CO_2 + C_3H_8) mixture were derived from the correlations of the perfect-gas heat capacity $C_{p,m}^{pg}$ given at Equation (9) and the estimated second acoustic virial coefficients β_a listed in Table 8 by a non-linear regression fitting to two different effective intermolecular potentials $U(r)$, as described in detail in [31]. As B determination is not initially very sensitive to the intermolecular potential used, two common spherical symmetric effective potentials for non-polar molecules were chosen such as the hard-core square well (HCSW):

$$\begin{aligned} U(r) &= \infty && r < \sigma_{SW} \\ U(r) &= -\varepsilon_{SW} && \sigma_{SW} \le r \le g\sigma_{SW} \\ U(r) &= 0 && r > g\sigma_{SW} \end{aligned} \tag{6}$$

and the Lennard-Jones (12,6) (LJ (12,6)):

$$U(r) = 4\varepsilon_{LJ}\left[\left(\frac{\sigma_{LJ}}{r}\right)^{12} - \left(\frac{\sigma_{LJ}}{r}\right)^{6}\right] \tag{7}$$

whose integration to derive B can be expressed as analytical close form in terms of modified Bessel functions of the first kind [50]. This procedure should be sufficient to perform the regression within our experimental expanded (k = 2) uncertainty $U(\beta_a)$. Here, σ_{Sw} is the hard-core length, ε_{Sw} is the square well depth, and g is σ_{Sw} times the length of the square well, whereas σ_{LJ} is the separation at which $U(r) = -\varepsilon_{LJ}$ and ε_{LJ} is the depth of the potential well.

The fitting parameters of the regression to the HCSW and LJ (12,6) effective potentials are listed in Table 9 with the Δ_{RMS} of the residuals of each fitting.

Table 9. Regression parameters of the hard-core square well (HCSW) and Lennard-Jones (LJ (12,6)) effective intermolecular potentials $U(r)$ and the root mean square (Δ_{RMS}) of the residuals of the fitting. σ_{SW} is the hard-core length, ε_{SW} is the well depth, g_{SW} is σ_{SW} times the length of the square well. σ_{LJ} is the separation at which $U(r) = -\varepsilon_{LJ}$ and ε_{LJ} is the depth of the potential well.

HCSW				LJ (12,6)		
σ_{SW} / Å	g_{SW}	ε_{SW} / eV	Δ_{RMS} of residuals / %	σ_{LJ} / Å	ε_{LJ} / eV	Δ_{RMS} of residuals / %
(0.60 CO_2 + 0.40 C_3H_8)						
41.821	1.5803	0.018227	0.27	4.9112	0.017492	0.49
(0.80 CO_2 + 0.20 C_3H_8)						
33.315	1.3695	0.033674	0.40	4.5438	0.017395	1.5

Results of B_{exp}, whose estimated mean expanded (k = 2) uncertainty is $U(B_{exp})$ = 1.1 % using the Monte Carlo method [45], are compared to predictions using the GERG-2008 EoS [10,11] in Figure 8 and Table 10. Hereafter, the comparison with the AGA8-DC92 EoS [13,14] is discarded due to the high disagreement with this model, with relative deviations of 9.0 % at best.

Table 10. Second density virial coefficient B and interaction second density virial coefficient B_{12} at the experimental temperatures from the deductions of the hard-core square well

(HCSW) and Lennard-Jones (LJ (12,6)) effective intermolecular potentials $U(r)$ for the (CO_2 + C_3H_8) mixtures, together with their corresponding relative expanded (k = 2) uncertainties.

	(0.60 CO_2 + 0.40 C_3H_8)			(0.80 CO_2 + 0.20 C_3H_8)			Average values by the HCSW potential for the two mixtures		
T / K	B_{HCSW} / $cm^3 \cdot mol^{-1}$	B_{LJ} / $cm^3 \cdot mol^{-1}$	$10^2 \cdot U(B)$	B_{HCSW} / $cm^3 \cdot mol^{-1}$	B_{LJ} / $cm^3 \cdot mol^{-1}$	$10^2 \cdot U(B)$	B_{12} / $cm^3 \cdot mol^{-1}$	$10^2 \cdot U(B_{12})$	$10^2 \cdot \Delta B_{12,GERG}$
273.16	−225.5	−221.8	1.1	−186.1	−173.8	0.54	−211.5		−1.36
300.00	−186.1	−184.8	1.3	−149.3	−144.7	0.60	−172.5		−0.57
325.00	−157.0	−156.9	1.4	−123.7	−122.8	0.66	−144.3	2.8	0.01
350.00	−133.4	−133.7	1.6	−103.6	−104.6	0.72	−121.6		0.53
375.00	−113.7	−114.2	1.8	−87.6	−89.2	0.80	−103.1		1.11

As can be seen in Figure 8, our results are more consistent with the GERG-2008 EoS [10,11] for the deductions from the HCSW and for the mixture with lower molar fraction of propane. The absolute average deviations are Δ_{AAD} (GERG) = (1.1 and 0.5) % for the mixtures (0.60 CO_2 + 0.40 C_3H_8) and (0.80 CO_2 + 0.20 C_3H_8), respectively, within $U(B_{exp})$ at all the temperature range studied for the latter mixture. This, along with the fact that the Δ_{RMS} of the residuals for the fitting from the LJ (12,6) potential are as high as 1.5 % and outside $U(\beta_a)$ for the mixture (0.80 CO_2 + 0.20 C_3H_8), leads us to neglect the B_{exp} values obtained from this effective potential for the determination of the interaction second density virial coefficients B_{12}:

$$B_{12} = \left[B_{exp} - \left(x_1^2 B_{11} + x_2^2 B_{22} \right) \right] \Big/ \left(2 x_1 x_2 \right) \quad (8)$$

Here, B_{11} is the second density virial coefficient of pure carbon dioxide of mole fraction x_1 and B_{22} is the second density virial coefficient of pure propane of mole fraction x_2, obtained from the corresponding equations of state [51] for pure carbon dioxide and [49] for pure propane, with estimated expanded (k = 2) uncertainties $U(B_{11})$ = 0.5 % and $U(B_{22})$ = 2.0 %, respectively [52].

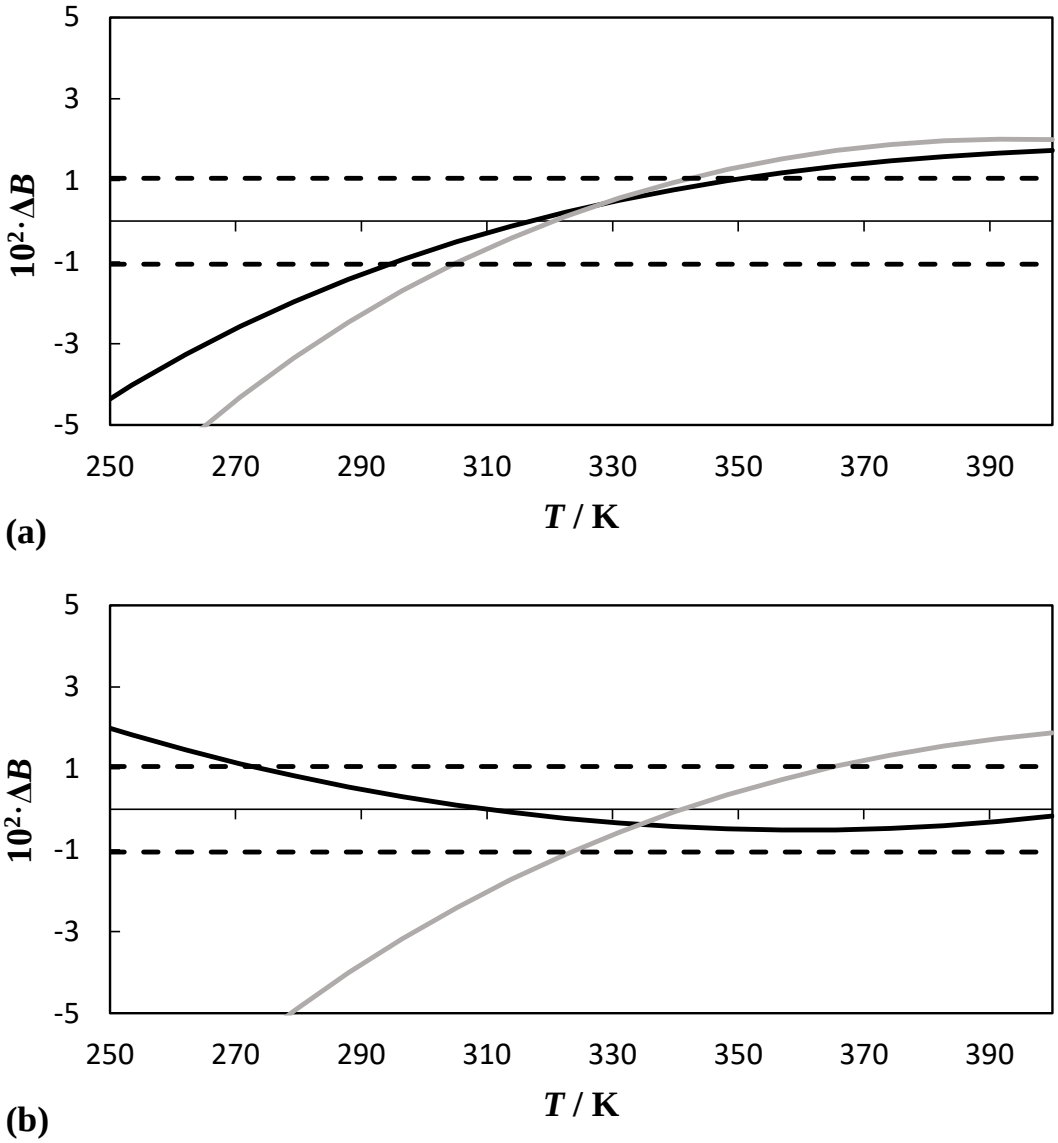

Figure 8. Relative deviations of the second density virial coefficient $\Delta B = (B_{exp} - B_{ref})/B_{ref}$ from GERG-2008 EoS [6,7], as a function of temperature for (a) the (0.60 CO_2 + 0.40 C_3H_8) mixture and (b) the (0.80 CO_2 + 0.20 C_3H_8) mixture using HCSW (black line) and LJ (12,6) (grey line) effective intermolecular potentials. Dashed lines depict the mean expanded (k = 2) uncertainty of this work

The relative deviations of cross second virial coefficient,$(B_{12,exp} - B_{12,ref})/B_{12,ref}$, from the GERG-2008 EoS [10,11] and the literature data are depicted in Figure 9.

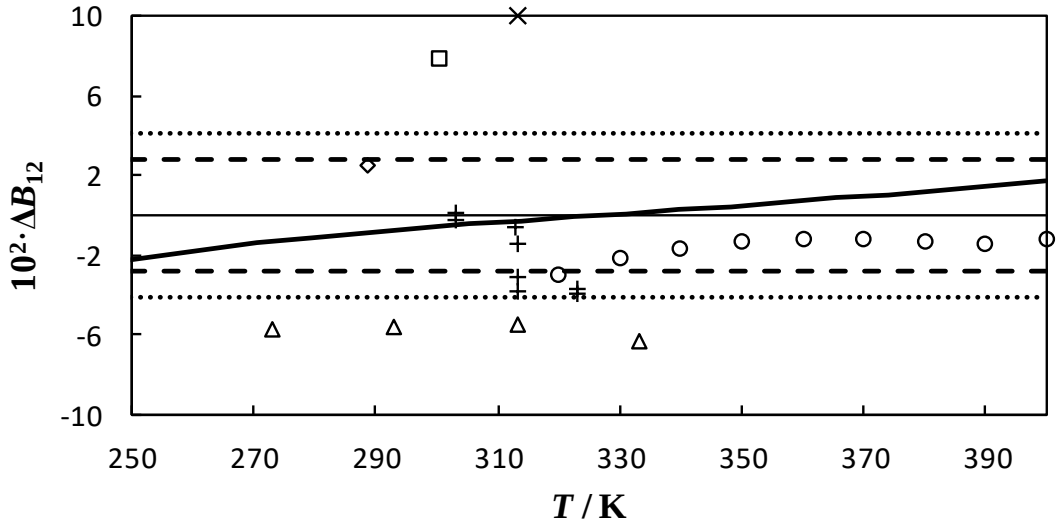

Figure 9. Relative deviations of the interaction second density virial coefficient $\Delta B_{12} = (B_{12,exp} - B_{12,ref})/B_{12,ref}$ as function of temperature, with $B_{12,exp}$ obtained from the average of the HCSW deductions for the two (CO_2 + C_3H_8) mixtures: solid line from the GERG-2008 EoS [10,11], △ Jaeschke et al. [53], ◇ Mason et al. [54], □ Bougard et al. [55], ＋ McElroy et al. [56], × Sie et al. [57], ○ Feng et al. [58]. Dashed lines depict the mean expanded (k = 2) uncertainty of this work and dotted lines depict the average expanded (k = 2) uncertainty of literature.

$B_{12,exp}$ were obtained from the average of the results derived by the HCSW effective intermolecular potential for the two (CO_2 + C_3H_8) mixtures. The literature data include values reported by Jaeschke et al. [53], Mason et al. [54], Bougard et al. [55], McElroy et al. [56], Sie et al. [57], and Feng et al. [58] which were obtained by different techniques such as densimeters based on the Archimedes principle, expansion techniques or Burnett method, and gas chromatography. Comparison to the GERG-2008 EoS [10,11] is performed to the average predicted values from the EoS for the two studied mixtures because, although B_{12} is only a function of the temperature, the reference model shows a slight dependence with the composition. The estimated expanded (k = 2) uncertainty $U(B_{12,exp})$ = 2.8 %, for the experimental values is similar to the mean of the literature values $U(B_{12,Literature})$ = 4.1 %. As

depicted in Figure 9, the discrepancies of our results $B_{12,exp}$ from the GERG-2008 EoS [10,11] are explained within $U(B_{12,exp})$, while the values of Sie et al. [57] and Bougard et al [55] are not in agreement with ours neither with the model nor with the other authors. In addition, the values of Mason et al. [54] and McElroy et al. [56] are in agreement within the mutual uncertainty of the literature and the experimental one with our estimations. Furthermore, the most recent results of Feng et al. [58] show a nearly constant discrepancy with our values in all the temperature range, but within the limit of the experimental uncertainty. Finally, the data set of Jaeschke et al. [53] deviates by about −6 % for all the isotherms. The overall absolute average deviation of the experimental B_{12} of this work from the literature data, discarding the outlier values of Sie et al. [59] and Bougard et al [57], is Δ_{AAD} = 2.4 % which is reasonable in comparison to its uncertainty.

4.4 Phase Equilibria.

Experimental phase equilibria data are compared to the predicted values of GERG-2008 equation [10,11] as is listed in Tables 5 and 6 shown above and they are also depicted in Figure 10.

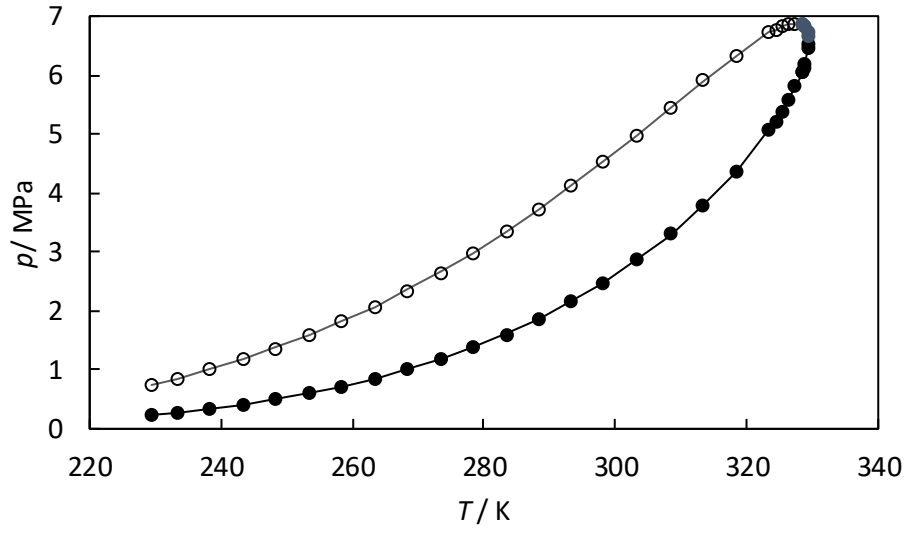

(a)

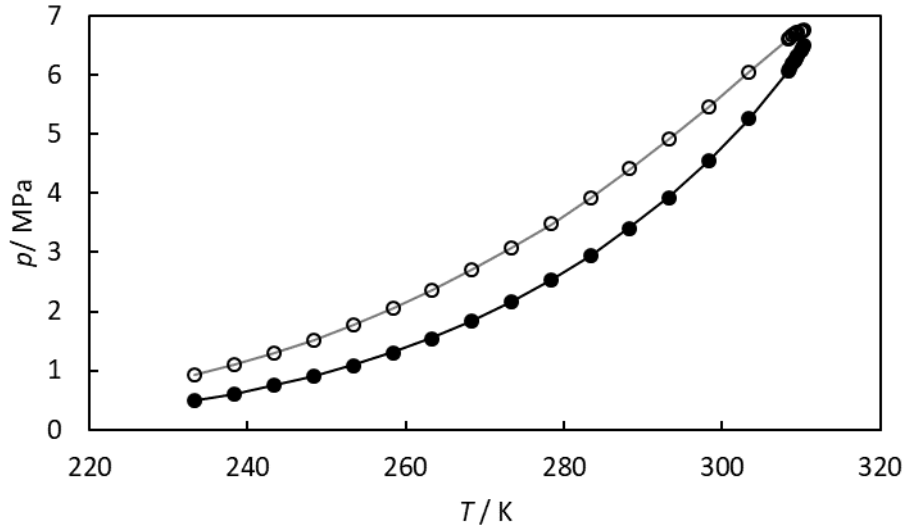

(b)

Figure 10: Phase envelope: a) the (0.60 CO_2 + 0.40 C_3H_8) mixture b) the (0.80 CO_2 + 0.80 C_3H_8) mixture. (o) bubble points; (•) retrograde dew points (•) dew points; (–) calculated bubble points using GERG-2008 EoS; (–) calculated dew points using GERG-2008. EoS [11]

The average absolute relative pressure deviations are 0.19% and 0.23% for bubble points and dew points, respectively, for the (0.60 CO_2 + 0.40 C_3H_8) mixture and 0.28% and 0.22% for bubble points and dew points of the (0.80 CO_2 + 0.20 C_3H_8) mixture. All these values are below the equation of state uncertainty which is estimated between 1% to 3% [11]. As seen, the (0.60 CO_2 + 0.40 C_3H_8) mixture presents a retrograde condensation zone, according to the critical point (327.71 K, 6.8724 MPa) calculated with the GERG-2008 equation, which has also been determined experimentally.

In addition, experimental results are also compared with the scarce literature data [61-64]. These data were selected between those whose compositions are close to our mixtures. Figure 11 presents the relative deviations between the different sets of experimental pressures and the corresponding values calculated using the GERG-2008 EoS [10,11].

This figure clearly shows that our deviations are much lower than the deviations obtained for the literature data, and our results scatter around the zero value and do not show any tendency.

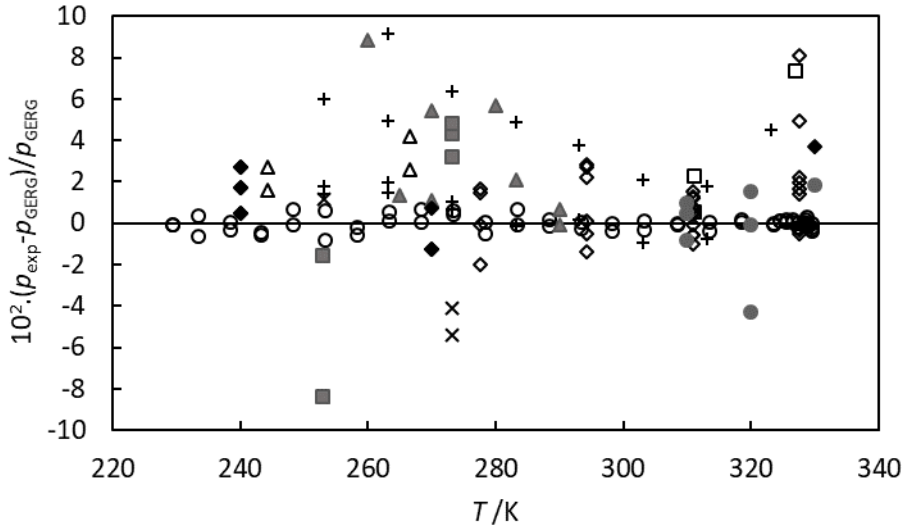

(a)

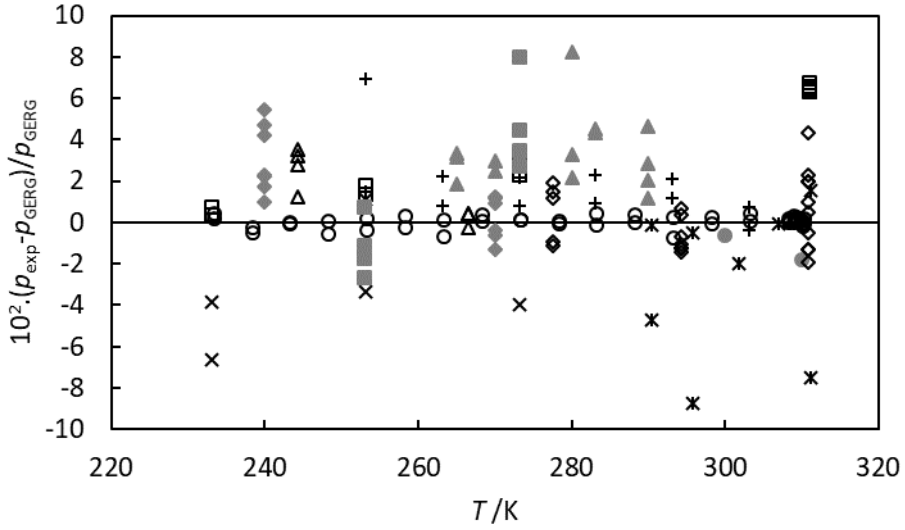

(b)

Figure 11. Relative deviations of pressure for (CO_2 + C_3H_8) mixtures: (a) x_{CO2}≈0.6; (b) x_{CO2}≈0.8. Symbols: (o) this work; (×) Akers et al. [61]; (Δ) Hamman et al. [62]; (□) Niesen et al. [63]; (+) Kim et al. [64]; (◊) Reamer et al. [65]; (■) Nagahama et al. [66]; (♦) Yucelen et al. [67]; (▲) Tanaka et al. [68]; (●) Nagata et al. [69]; (⋇)Poettmann et al. [70].

The average absolute relative deviations obtained for the x_{CO2}≈0.6 (CO_2 + C_3H_8) mixture are: 3.91% for data from [61], 2.77% for [62], 4,63% for [63], 2.83% for [64], 1.53% for [65], 4.48% for [66], 1.67% for [67], 3.93% for [68], 1.43% for [69]. Lower deviations (in general) were found for the x_{CO2}≈0.8 (CO_2 + C_3H_8) mixture: 3.78% for [61], 1.70% for [62], 2.27% for [63], 1.83% for [64], 1.38% for [65], 2.95% for [66], 2.09% for [67], 3.95% for [68],

1.21% for [69], 4.72% for [70]. These values are mostly in agreement with the uncertainty of the EoS.

One of the main advantages of our technique is that the composition is fixed and its uncertainty is lower than other techniques where the composition is measured. As is indicated in [11], the main contribution to phase equilibria uncertainty is due to the composition uncertainty.

5. Conclusions.

New high-accurate experimental speed of sound and phase equilibria data for two binary mixtures of carbon dioxide and propane, with nominal compositions of mixtures (0.60 CO_2 + 0.40 C_3H_8) and (0.80 CO_2 + 0.20 C_3H_8) are reported. Speed of sound measurements were performed with an acoustic stainless-steel spherical resonator achieving an expanded (k = 2) uncertainty of 250 parts in 10^6 (0.025 %).

From these data, perfect-gas heat capacity ratios and heat capacities were obtained with an expanded (k = 2) uncertainty between (0.15 to 0.28) %, second acoustic virial coefficients were deduced with an expanded (k = 2) uncertainty of (0.33 to 1.1) %, and third acoustic virial coefficients were determined with an expanded (k = 2) uncertainty of (2.4 to 35) %. Speed of sound results are consistent within the large stated 1% uncertainty of reference models AGA8-DC92 Eos [13,14] and GERG-2008 EoS [10,11], with deviations that increase towards higher pressures, showing a better agreement in the order of 0.06 % according to the latter equation of state at high pressures. On the contrary, the comparison of the derived heat capacities in the limit of zero pressure is more satisfactory with respect to the AGA8-DC92 EoS [13,14], yielding deviations less than 0.1 %.

The low uncertainty of the acoustic virial coefficients allows us to analyze our data using the effective intermolecular potentials of hard-core square well and Lennard-Jones (12,6) in order

to derive second density virial coefficients and the corresponding interaction coefficients for this binary mixture. The relative differences of the interaction second density virial coefficient are consistent regarding to the GERG-2008 EoS [10,11] and within the claimed uncertainty of most authors in the literature, with deviations less than 5 % in comparison with an experimental expanded (k = 2) uncertainty of 2.8 %.

Finally, phase equilibria data, measured using a cylindrical microwave resonator, allow accurate bubble or dew points with expanded uncertainties (k = 2) (40 mK and $4.0 \cdot 10^{-4}$ (p/Pa) + 1400 Pa). The deviations obtained from GERG-2008 EoS [10,11] are lower than the uncertainty of the EoS.

This work tries to enrich the set of accurate data and to fill the gap that exists for binary mixtures composed of carbon dioxide and propane, which will benefit the development of improved correlations for the reference equations of state and, hence, the calculations made during the design and control stages of the mentioned process involving these mixtures, where precise and accurate information of the thermodynamic properties is required for the understanding of the whole system.

Acknowledgements.

This work was supported by FEDER/Ministerio de Ciencia, Innovación y Universidades – Agencia Estatal de Investigación (Project ENE2017-88474-R) and FEDER/Junta de Castilla y León (Project VA280P18).

References.

[1] Niu B, Zhang Y. Experimental study of the refrigeration cycle performance for the R744/R290 mixtures. Int J Refrig 2007;30:37–42. https://doi.org/10.1016/j.ijrefrig.2006.06.002.

[2] Kim JH, Cho JM, Kim MS. Cooling performance of several CO2/propane mixtures

and glide matching with secondary heat transfer fluid. Int J Refrig 2008;31:800–6. https://doi.org/10.1016/j.ijrefrig.2007.11.009.

[3] Garg P, Kumar P, Srinivasan K, Dutta P. Evaluation of carbon dioxide blends with isopentane and propane as working fluids for organic Rankine cycles. Appl Therm Eng 2013;52:439–48. https://doi.org/10.1016/j.applthermaleng.2012.11.032.

[4] Feng L, Zheng D, Chen J, Dai X, Shi L. Exploration and Analysis of CO2 + Hydrocarbons Mixtures as Working Fluids for Trans-critical ORC. Energy Procedia 2017;129:145–51. https://doi.org/10.1016/j.egypro.2017.09.191.

[5] Illés V, Szalai O, Then M, Daood H, Perneczki S. Extraction of hiprose fruit by supercritical CO2 and propane. J Supercrit Fluids 1997;10:209–18. https://doi.org/10.1016/S0896-8446(97)00018-1.

[6] King JW, Holliday RL, List GR, Snyder JM. Hydrogenation of vegetable oils using mixtures of supercritical carbon dioxide and hydrogen. JAOCS, J Am Oil Chem Soc 2001;78:107–13. https://doi.org/10.1007/s11746-001-0229-8.

[7] Palla C, Hegel P, Pereda S, Bottini S. Extraction of jojoba oil with liquid CO2 + propane solvent mixtures. J Supercrit Fluids 2014;91:37–45. https://doi.org/10.1016/j.supflu.2014.04.005.

[8] Correa M, Mesomo MC, Pianoski KE, Torres YR, Corazza ML. Extraction of inflorescences of Musa paradisiaca L. using supercritical CO2 and compressed propane. J Supercrit Fluids 2016;113:128–35. https://doi.org/10.1016/j.supflu.2016.03.016.

[9] Luo P, Zhang Y, Wang X, Huang S. Propane-enriched CO 2 immiscible flooding for improved heavy oil recovery. Energy and Fuels 2012;26:2124–35. https://doi.org/10.1021/ef201653u.

[10] Kunz O, Klimeck R, Wagner W, Jaeschke M. GERG Technical Monograph 15 (2007) The GERG-2004 wide-range equation of state for natural gases and other

mixtures. 2007.

[11] Kunz O, Wagner W. The GERG-2008 wide-range equation of state for natural gases and other mixtures: An expansion of GERG-2004. J Chem Eng Data 2012;57:3032–91. https://doi.org/10.1021/je300655b.

[12] Lin CW, Trusler JPM. Speed of sound in (carbon dioxide + propane) and derived sound speed of pure carbon dioxide at temperatures between (248 and 373) K and at pressures up to 200 MPa. J Chem Eng Data 2014;59:4099–109. https://doi.org/10.1021/je5007407.

[13] Committee TM. AGA Report No. 8 Part 2 Thermodynamic Properties of Natural Gas and Related Gases 2017.

[14] ISO 20765-1:2005. Natural gas - Calculation of thermodynamic properties. Part 1: Gas phase properties for transmission and distribution applications 2005.

[15] Susial R, Gómez-Hernández A, Lozano-Martín D, del Campo D, Martín MC, Segovia JJ, A novel technique based in a cylindrical microwave resonator for high pressure phase equilibrium determination, J. Chem. Thermodyn. 2019;35:124–132. doi:10.1016/j.jct.2019.03.027.

[16] International Organisation for Standardization. Gas analysis — Preparation of calibration gas mixtures — Part 1: Gravimetric method for Class I mixtures. 2014.

[17] International Organization for Standardization. Gas analysis - Comparison methods for determining and checking the compposition of calibration gas mixtures. 2006.

[18] Lemmon EW, Bell IH, Huber ML, McLinden MO. NIST Standard Reference Database 23: Reference Fluid Thermodynamic and Transport Properties-REFPROP, Version 10.0, National Institute of Standards and Technology 2018:135. https://doi.org/https://doi.org/10.18434/T4/1502528.

[19] Span R, Wagner W. A new equation of state for carbon dioxide covering the fluid region from the triple-point temperature to 1100 K at pressures up to 800 MPa. J

Phys Chem Ref Data 1996;25:1509–96. https://doi.org/10.1063/1.555991.

[20] Lemmon EW, McLinden MO, Wagner W. Thermodynamic properties of propane. III. A reference equation of state for temperatures from the melting line to 650 K and pressures up to 1000 MPa. J Chem Eng Data 2009;54:3141–80. https://doi.org/10.1021/je900217v.

[21] Pérez-Sanz FJ, Segovia JJ, Martín MC, Del Campo D, Villamañán MA. Speeds of sound in (0.95 N2 + 0.05 CO and 0.9 N2 + 0.1 CO) gas mixtures at T = (273 and 325) K and pressure up to 10 MPa. J Chem Thermodyn 2014;79:224–229. https://doi.org/10.1016/j.jct.2014.07.022.

[22] Lozano-Martín D, Rojo A, Martín MC, Vega-Maza D, Segovia JJ. Speeds of sound for (CH4 + He) mixtures from p = (0.5 to 20) MPa at T = (273.16 to 375) K. J Chem Thermodyn 2019;139:105839. https://doi.org/10.1016/j.jct.2019.07.011.

[23] Mehl JB. Analysis of resonance standing-wave measurements. J Acoust Soc Am 1978;64:1523–5. https://doi.org/10.1121/1.382096.

[24] Ewing MB, Trusler JPM. On the analysis of acoustic resonance measurement. J Acoust Soc Am 1989;85:1780–2. https://doi.org/10.1121/1.397970.

[25] Pérez-Sanz FJ, Martín MC, Chamorro CR, Fernández-Vicente T, Segovia JJ. Heat capacities and acoustic virial coefficients for a synthetic coal mine methane mixture by speed of sound measurements at T = (273.16 and 250.00) K. J Chem Thermodyn 2016;97:137–41. https://doi.org/10.1016/j.jct.2016.01.020.

[26] Lozano-Martín D, Segovia JJ, Martín MC, Fernández-Vicente T, del Campo D. Speeds of sound for a biogas mixture CH_4 + N_2 + CO_2 + CO from p = (1–12) MPa at T = (273, 300 and 325) K measured with a spherical resonator. J Chem Thermodyn 2016;102:348–56. https://doi.org/10.1016/j.jct.2016.07.033.

[27] Segovia JJ, Lozano-Martín D, Martín MC, Chamorro CR, Villamañán MA, Pérez E, et al. Updated determination of the molar gas constant R by acoustic measurements in

argon at UVa-CEM. Metrologia 2017;54:663–73. https://doi.org/10.1088/1681-7575/aa7c47.

[28] Preston-Thomas H. The International temperature scale of 1990 (ITS-90). Metrologia 1990;27:3–10. https://doi.org/10.1088/0026-1394/27/1/002.

[29] Preston-Thomas H. The International Temperature Scale of 1990 (ITS-90). Metrologia 1990;27:107–107. https://doi.org/10.1088/0026-1394/27/2/010.

[30] Mehl JB, Moldover MR. Precondensation phenomena in acoustic measurements. J Chem Phys 1982;77:455–65. https://doi.org/10.1063/1.443627.

[31] Lozano-Martín D, Martín MC, Chamorro CR, Tuma D, Segovia JJ. Speed of sound for three binary (CH_4 + H_2) mixtures from p = (0.5 up to 20) MPa at T = (273.16 to 375) K. Int J Hydrogen Energy 2019. https://doi.org/10.1016/j.ijhydene.2019.12.012.

[32] Estrada-Alexanders AF, Trusler JPM. Speed of sound in carbon dioxide at temperatures between (220 and 450) K and pressures up to 14 MPa. J Chem Thermodyn 1998;30:1589–601. https://doi.org/10.1006/jcht.1998.0428.

[33] Estrada-Alexanders AF, Hurly JJ. Kinematic viscosity and speed of sound in gaseous CO, CO2, SiF4, SF6, C4F8, and NH3 from 220 K to 375 K and pressures up to 3.4 MPa. J Chem Thermodyn 2008;40:193–202. https://doi.org/10.1016/j.jct.2007.07.002.

[34] Liu Q, Feng X, An B, Duan Y. Speed of sound measurements using a cylindrical resonator for gaseous carbon dioxide and propene. J Chem Eng Data 2014;59:2788–98. https://doi.org/10.1021/je500424b.

[35] Trusler JPM, Zarari MP. The speed of sound in gaseous propane at temperatures between 225 K and 375 K and at pressures up to 0.8 MPa. J Chem Thermodyn 1996;28:329–35. https://doi.org/10.1006/jcht.1996.0032.

[36] Hurly JJ, Gillis KA, Mehl JB, Moldover MR. The viscosity of seven gases measured with a Greenspan viscometer. Int J Thermophys 2003;24:1441–74.

https://doi.org/10.1023/B:IJOT.0000004088.04964.4c.

[37] Meier K, Kabelac S. Thermodynamic properties of propane. IV. Speed of sound in the liquid and supercritical regions. J Chem Eng Data 2012;57:3391–8. https://doi.org/10.1021/je300466a.

[38] Stephenson JC, Wood RE, Moore CB. Vibrational Relaxation of Laser-Excited CO_2 - Polyatomic Mixtures 2003;4813:1–5.

[39] Estela-Uribe JF, Trusler JPM, Chamorro CR, Segovia JJ, Martín MC, Villamañán MA. Speeds of sound in $\{(1 - x)CH_4 + xN_2\}$ with x = (0.10001, 0.19999, and 0.5422) at temperatures between 170 K and 400 K and pressures up to 30 MPa. J Chem Thermodyn 2006;38:929–37. https://doi.org/10.1016/j.jct.2005.10.006.

[40] Herzberg G. Molecular Spectra and Molecular Structure II. Infrared and Raman Spectra of polyatomic molecules. Toronto, New York, London: D. Van Nostrand Company; 1945.

[41] Shimanouchi T. Tables of Molecular Vibrational Frequences Consolidated, vol. 1. Natl Bur Stand 1972:1–16. https://doi.org/10.6028/NBS.NSRDS.39.

[42] Susial R, Gómez-Hernández A, Lozano-Martín D, del Campo D, Martín MC,. Segovia JJ. A novel technique based in a cylindrical microwave resonator for high pressure phase equilibrium determination. J. Chem. Thermodyn. 2019;135: 124–132. https://doi.org/10.1016/j.jct.2019.03.027.

[43] Martin E, Hernandez A, Sanchez MC, Zamarro JM, Margineda J. Automatic measurement of Q factor and resonant frequency of microwave resonators, J. Phys. E: Scientific Instruments 1981;14:961−962. https://doi.org/10.1088/0022-3735/14/8/016.

[44] JCGM. Evaluation of measurement data — Guide to the expression of uncertainty in measurement. 2008.

[45] JCGM. Evaluation of measurement data — Supplement 1 to the “Guide to the

expression of uncertainty in measurement" — Propagation of distributions using a Monte Carlo method. 2008.

[46] Fischer J, Fellmuth B, Gaiser C, Zandt T, Pitre L, Sparasci F, et al. The Boltzmann project. Metrologia 2018;55:R1–20. https://doi.org/10.1088/1681-7575/aaa790.

[47] Jaeschke M, Schley P. Ideal-gas thermodynamic properties for natural-gas applications. Int J Thermophys 1995;16:1381–92. https://doi.org/10.1007/BF02083547.

[48] Chao J, Wilhoit RC, Zwolinski BJ. Ideal Gas Thermodynamic Properties of Ethane and Propane. J Phys Chem Ref Data 1973;2:427–38. https://doi.org/10.1063/1.3253123.

[49] Lemmon EW, McLinden MO, Wagner W. Thermodynamic properties of propane. III. A reference equation of state for temperatures from the melting line to 650 K and pressures up to 1000 MPa. J Chem Eng Data 2009;54:3141–80. https://doi.org/10.1021/je900217v.

[50] Vargas P, Muñoz E, Rodriguez L. Second virial coefficient for the Lennard–Jones potential. Phys A Stat Mech Its Appl 2001;290:92–100. https://doi.org/10.1016/S0378-4371(00)00362-9.

[53] Span R, Wagner W. A new equation of state for carbon dioxide covering the fluid region from the triple-point temperature to 1100 K at pressures up to 800 MPa. J Phys Chem Ref Data 1996;25:1509–96. https://doi.org/10.1063/1.555991.

[54] Frenkel EM, Marsh KN. Virial Coefficients of Pure Gases. vol. 21A. Berlin/Heidelberg: Springer-Verlag; 2002. https://doi.org/10.1007/b71692.

[55] Jaeschke. M, Audibert. S, van Canegham. P, Humphreys. AE, Janssen-van Rosemalen. R, Pellei. Q, et al. GERG Tech. Monogr. TM2 - High Accuracy Compressibility factor Calculation for Natural Gases and Similar Mixtures by Use of a Truncated Virial Equation. Düsseldorf: 1989.

[56] Mason DMA, Eakin BE. Compressibility Factor of Fuel Gases at 60° F. and 1 Atm. J Chem Eng Data 1961;6:499–504. https://doi.org/10.1021/je60011a006.

[57] Bougard J, Jadot R. Second coefficient du viriel de mélanges binaires d'halocarbones. J Chim Phys 1976;73:415–7. https://doi.org/10.1051/jcp/1976730415.

[58] McElroy PJ, Kee LL, Renner CA. Excess Second Virial Coefficients for Binary Mixtures of Carbon Dioxide with Methane, Ethane, and Propane. J Chem Eng Data 1990;35:314–7. https://doi.org/10.1021/je00061a024.

[59] Sie ST, Van Beersum W, Rijnders GWA. High-Pressure Gas Chromatography and Chromatography with Supercritical Fluids. I. The Effect of Pressure on Partition Coefficients in Gas-Liquid Chromatography with Carbon Dioxide as a Carrier Gas. Sep Sci 1966;1:459–90. https://doi.org/10.1080/01496396608049460.

[60] Feng XJ, Liu Q, Zhou MX, Duan YY. Gaseous pvTx properties of mixtures of carbon dioxide and propane with the burnett isochoric method. J Chem Eng Data 2010;55:3400–9. https://doi.org/10.1021/je100148h.

[61] Akers WW, Kelley RE, Lipscomb TG. Carbon-dioxide propane system, Ind Eng Chem 1954;46:2535–2536. https://doi.org/10.1021/ie50540a039.

[62] Hamam SEM,. Lu BCY. Isothermal vapor-liquid equilibria in binary system propane-carbon dioxide, J Chem Eng Data 1976;21:200–204. https://doi.org/10.1021/je60069a020.

[63] Niesen VG, Rainwater JC. Critical locus, (vapor + liquid) equilibria, and coexisting densities of (carbon dioxide + propane) at temperatures from 311 K to 361 K, J Chem Thermodyn 1990;22:777–795. https://doi.org/10.1016/0021-9614(90)90070-7.

[64] Kim JH, Kim MS. Vapor-liquid equilibria for the carbon dioxide + propane system over a temperature range from 253.15 to 323.15 K, Fluid Phase Equilib 2005;239:13–19. https://doi.org/10.1016/j.fluid.2005.09.006.

[65] Reamer HH, Sage BH, Lacey WN. Phase equilibria in hydrocarbon systems: Volumetric and phase behavior of the propane - carbon dioxide system, Ind Eng Chem 1951;43: 2515–2520. https://doi.org/10.1021/ie50503a035.

[66] Nagahama K, Konishi H, Hoshino D, Hirata M. Binary vapor-liquid equilibria of carbon dioxide - light hydrocarbons at low temperature, J Chem Eng Jpn 1974;7: 323–328. https://doi.org/10.1252/jcej.7.323.

[67] Yucelen B, Kidnay AJ. Vapor-liquid equiliblria in the nitrogen + cCarbon dioxide + propane system from 240 to 330 K at pressures to 15 MPa, J Chem Eng Data 1999;44:926–931. https://doi.org/10.1021/je980321e.

[68] Tanaka K, Higashi Y, Akasaka R, Kayukawa Y, Fujii K. Measurements of the vapor-liquid equilibrium for the CO_2 + R290 mixture, J Chem Eng Data 2009; 54:1029–1033. https://doi.org/10.1021/je800938s.

[69] Nagata Y, Mizutani K, Miyamoto H. The precise measurement of the (vapour + liquid) equilibrium properties for (CO_2 + isobutane) binary mixtures, J Chem Thermodyn 2011;43:244–247. https://doi.org/10.1016/j.jct.2010.09.004.

[70] Poettmann FH, Katz DL. Phase behavior of binary carbon dioxide - paraffin systems, Ind Eng Chem 1945;37:847–853. https://doi.org/10.1021/ie50429a017.